ADHESION/DIFFUSION BARRIER LAYERS FOR COPPER INTEGRATION: CARBON-SILICON POLYMER FILMS AND TANTLUM SUBSTRATES

Li Chen, B.S., M.S.

Dissertation Prepared for the Degree of

DOCTOR OF PHILOSOPHY

UNIVERSITY OF NORTH TEXAS

December 1999

APPROVED:

Jeffry A. Kelber, Major Professor
Michael Richmond, Committee Member
Teresa Golden, Committee Member
David Wiedenfeld, Committee Member
Ruthanne D. Thomas, Chair of the Department of Chemistry
C. Neal Tate, Dean of the Robert B. Toulouse School of Graduate Studies

Chen, Li, Adhesion/diffusion barrier layers for copper integration: carbon-silicon polymer films and tantalum substrates. Doctor of Philosophy (Chemistry), December 1999, 98 pp., 5 tables, 37 illustrations, references, 138 titles.

The Semiconductor Industry Association (SIA) has identified the integration of copper (Cu) with low-dielectric-constant (low-k) materials as a critical goal for future interconnect architectures. A fundamental understanding of the chemical interaction of Cu with various substrates, including diffusion barriers and adhesion promoters, is essential to achieve this goal. The objective of this research is to develop novel organic polymers as Cu/low-k interfacial layers and to investigate popular barrier candidates, such as clean and modified tantalum (Ta) substrates.

Carbon-silicon (C-Si) polymeric films have been formed by electron beam bombardment or ultraviolet (UV) radiation of molecularly adsorbed vinyl silane precursors on metal substrates under ultra-high vacuum (UHV) conditions. Temperature programmed desorption (TPD) studies show that polymerization is via the vinyl groups, while Auger electron spectroscopy (AES) results show that the polymerized films have compositions similar to the precursors. Films derived from vinyltrimethyl silane (VTMS) are adherent and stable on Ta substrates until 1100 K. Diffusion of deposited Cu overlayers is not observed below 800 K, with dewetting occurred only above 400 K. Hexafluorobenzene moieties can also be incorporated into the growing film with good thermal stability.

Studies on the Ta substrates demonstrate that even sub-monolayer coverages of oxygen or carbide on polycrystalline Ta significantly degrade the strength of Cu/Ta

chemical interactions, and affect the kinetics of Cu diffusion into bulk Ta. On clean Ta, monolayer coverages of Cu will de-wet only above 600 K. A partial monolayer of adsorbed oxygen (3L O_2 at 300 K) results in a lowering of the de-wetting temperature to 500 K, while saturation oxygen coverage (10 L O_2, 300 K) results in de-wetting at 300 K. Carbide formation also lowers the de-wetting temperature to 300 K. Diffusion of Cu into the Ta substrate at 1100 K occurs only after a 5-minute induction period. This induction period increases to 10 min for partially oxidized Ta, 15 min for carbidic Ta and 20 min for fully oxidized Ta.

ACKNOWLEDGMENTS

Financial support for this research was provided by the Semiconductor Research Corporation (SRC) through the Center for Advanced Interconnect Science and Technology (CAIST), and is gratefully acknowledged.

TABLE OF CONTENTS

LIST OF TABLES

LIST OF ILLUSTRATIONS

Table Page

CHAPTER 1

INTRODUCTION

The semiconductor industry is experiencing the transition from aluminum-alloy to copper-based interconnects as microelectronic device dimensions continue to shrink (1). As devices approach the sub-quarter-micron era, the reliability of existing Al technology becomes questionable. The major limitations of Al consist of two factors: one is stress-voiding induced circuit failure associated with electromigration (2), the other is the high electrical resistivities of Al and its alloys. Cu has attracted attention as a new metallization material because of its superior resistance to electromigration and low bulk electrical resistivity. Cu interconnects provide several advantages over Al, which include the ability to reduce the number of metal levels, increase chip speed and minimize manufacturing costs (3). However, Cu is known to diffuse rapidly into Si and SiO_2, causing degradation to device. Also, its adhesion to Si and most dielectric films is poor. Consequently, diffusion barriers and adhesion promoters must be developed before Cu can be used in manufacturing devices (1, 4-12).

The research studies presented in this dissertation focus on the fundamental surface chemical interactions of Cu with potential adhesion/barrier materials. These studies include:

(1) The development of novel polymeric films that demonstrates excellent chemical stability and potential as ultra-thin Cu diffusion barriers.

(2) The studies of Cu adhesion, diffusion and nucleation behavior on polycrystalline Ta and the importance of surface impurities in controlling such phenomena.

The above studies were carried out under ultra-high vacuum (UHV) conditions. Surface analytical techniques, such as Auger electron Spectroscopy (AES) and temperature programmed desorption (TPD), were employed.

This dissertation consists of three chapters. The first chapter provides background information on the interconnect integration, namely, role of time delay and the necessity of Cu and low-dielectric-constant materials, as well as experimental methodology. Chapter 2 presents the studies on the formation of polymeric carbon-silicon on metal substrates. Chapter 3 discusses the effect of surface impurities on the copper/tantalum interface.

1.1. RC Delay

The semiconductor industry has maintained its growth by achieving a 25-30% cost reduction per function per year throughout its history (1). Such rapid progress in integrated circuits (ICs) has been maintained by design innovation, device shrinkage, wafer size increase, yield improvement and equipment utilization improvements (1). Historically, the largest contribution to productivity growth has been the reduction in feature size. As the basic device dimension (transistor gate length) decreases, the carrier transient time at a given voltage across the gate also decreases, making it a faster device.

This scaling increases not only the speed of the circuits but also the number of transistors per unit area in an IC, making it more cost-efficient. The signal propagation to and from the device, however, must occur through the interconnections between different areas. These charge carrying devices are Cu or Al wires, which are insulated from each other by dielectrics. Figure 1.1 shows (a) the schematic diagram of a basic Cu interconnect structure and (b) the cross section of a multilayer interconnect structure with six levels of Cu wires/vias (13).

(a)

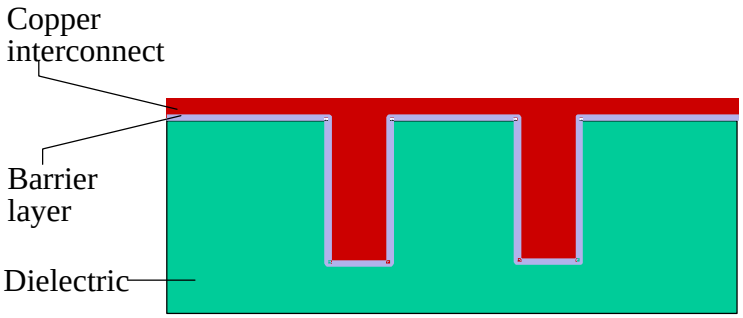

(b)

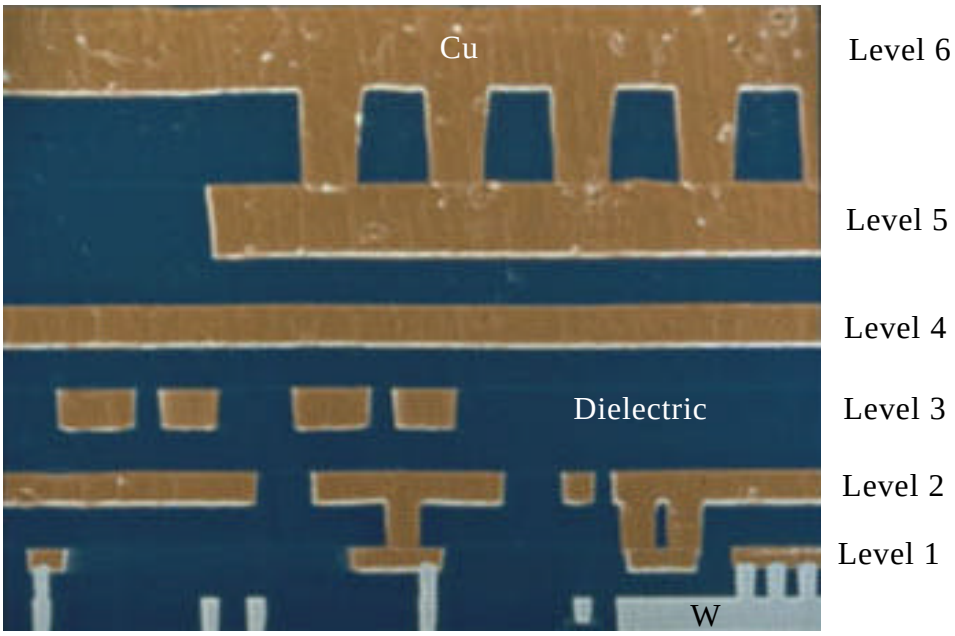

Figure 1.1. (a) Schematic diagram of a basic Cu interconnect structure; (b) scanning electron microscopy (SEM) cross section of a multilayer interconnect structure with six levels of Cu wires/vias (13).

Smaller wire dimension due to scaling causes an increase in the effective total resistance (R) of the metal lines. Narrower interline spacing also increases the effective total capacitance (C) between the lines. The overall effect is the so-called RC delay (4, 5, 8, 14-16). The RC delay can be approached by multiplying R with a simple plate capacitance, giving the following expression (4, 5):

$$RC = \frac{\rho}{t_M}\frac{L^2\varepsilon_{ILD}}{t_{ILD}} \qquad (1\text{-}1)$$

where ρ, t_M, and L are the resistivity, thickness and length of the metal repectively, while ε_{ILD} and t_{ILD} are the permittivity and thickness of the interlayer dielectrics (ILD).

Jeng et al. (8) have investigated the interconnect RC delay and the intrinsic gate daly as a function of IC feature sizes. The results of their studies are shown in Figure 1.2. When the device geometry is large (> 1 μm), circuit performance is almost completely limited by intrinsic gate delay. While the intrinsic delay continues to improve through scaling, the interconnect RC delay becomes the dominant component in the sub-micron regions.

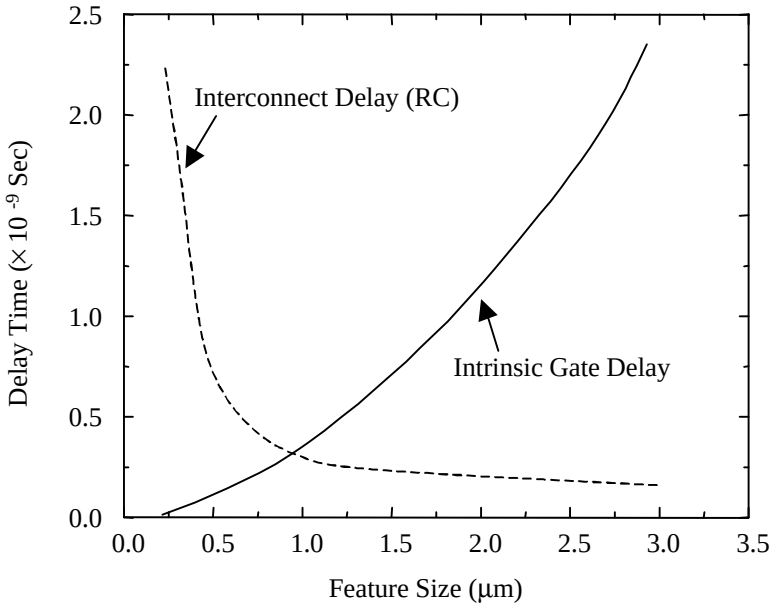

Figure 1.2. Delay time as a function of feature size

The rapid increase in RC delay time due to scaling, makes it the performance-limiting factor for ICs with feature size < 0.25 μm. To address this problem, new materials for use as metal lines and interlayer dielectrics (ILD), as well as alternative architectures, have been proposed to replace the current aluminum and silicon dioxide interconnect technology.

The simplified estimate of RC delay, as described in Equation (1-1), gives direct options to solve the problem. Reducing resistivity (ρ) and length (L) of the metal line, as well as interlayer dielectric permittivity (ε_{ILD}), will minimize the RC time constant. This means switching to metals with better conductivity (e.g., Cu), ILDs with lower dielectric

constants (e.g., Teflon), and reduced interconnection lengths (e.g., multilevel architectures rather than simple level planar interconnections).

Significant effort will be required to successfully integrate new materials into chip products at low cost and high yield. Meeting demands within expected time frame, as specified in Table 1.1 by the Technology Roadmap for Semiconductors (1), will be the most significant challenge for the interconnect area.

Table 1.1. Roadmap for interconnect technology requirements

Year	**1997**	**1999**	**2001**	**2003**	**2006**	**2009**	**2012**
Feature size (μm)	0.25	0.18	0.15	0.13	0.10	0.07	0.05
Metal levels	6	6-7	7	7	7-8	8-9	9
Interconnect length (m/chip)	820	1,480	2,160	2,840*	5,140*	10,000**	24,000**
Metal dimension (nm)	250	180	150	130*	100*	70*	50*
Barrier/cladding thickness (nm)	100	23*	20*	16*	11*	8**	6**
Metal resistivity (μΩ-cm)	3.3	2.2*	2.2*	2.2*	2.2*	< 1.8**	< 1.8**
Dielectric constant (k)	3.0-4.1	2.5-3.0*	2.0-2.5*	1.5-2.0*	1.5-2.0*	≤ 1.5**	≤ 1.5**

Notes: * Solution being pursued, ** No known solution

1.2. Copper Metallization for Interconnection Technology

Formation of metal lines on electronic devices or integrated circuits has been referred to as metallization. The term “interconnection” or “interconnect” is used instead when metals are specifically used as interconnecting wires (4).

A comparison of Al to some other low-resistivity metals that are potential replacements is listed in Table 1.2 (4-6).

Table 1.2. Properties of possible interconnect metals

Property		Metal				
		Al	Cu	Ag	Au	W
Resistivity (μΩ-cm)		2.66	1.67	1.59	2.35	5.65
Melting point (°C)		660	1085	962	1064	3387
Electromigration resistance		Low	High	Very low	Very high	Very high
Corrosion in air		Low	High	High	Very low	Low
Adhesion to SiO_2		Good	Poor	Poor	Poor	Poor
Deposition	sputtering	Yes	Yes	Yes	Yes	Yes
	Evaporation	Yes	Yes	Yes	Yes	Yes
	CVD	Yes	Yes	?	?	Yes
Etching	Dry	Yes	?	?	?	Yes
	Wet	Yes	Yes	Yes	Yes	Yes

Al has been extensively used as the interconnection metal because of its relatively low resistivity and good corrosion resistance in air. Another important reason is its ability to reduce interfacial SiO_2 and form strong chemical bonding with the underlying silicon/oxide substrate. This accounts for the excellent adhesion ability to SiO_2 that is not shared by the other four metals. However, in view of its low melting point and electromigration related issues, replacement of Al is inevitable for ULSI applications.

Electromigration is the movement of interconnection material in the direction of electron flow because of momentum transfer from electrons to the metal ions (17). It is noticeable only when current density is very high ($> 10^5$ A/cm^2), as is often the case in ICs. The effects of such migration are the growth of hillocks toward the positive end and the formation of voids and ultimately a break near the negative end. Currently this detrimental effect is lessened by doping Al with small amounts (1-2%) of Cu (17). As the line width continues to shrink in ULSI applications, the current density will keep increasing. The reliability of the circuits calls for the complete replacement of Al.

Of the five metals, W has the highest resistivity, even though it offers high-temperature stability, good corrosion resistance, excellent electromigration resistance, practical deposition methods and etching patternability. This major drawback, together with the poor adhesion ability to SiO_2, makes extensive utilization of W in high-performance interconnects unlikely.

Applications of Ag and Au to replace Al have been suggested in the last three decades (4). The only advantage of Ag is its resistivity, about 5% lower that that of Cu. But, besides a poor electromigration resistance, it is more costly than Cu, and is reported to diffuse into SiO_2 at a much faster rate than Cu, especially under bias (18). Au also offers only one advantage over Cu – its excellent corrosion resistance. But it is worse than Ag and W in the aspect of adhesion to dielectric surfaces. It is far more costly and its electromigration behavior is inferior to Cu (4).

It can be clearly seen from the above discussions that Cu is the best choice for the advanced multilevel metallization applications. However, some critical issues need to be

resolved in order for Cu technology to become an industrial reality. As mentioned previously, Cu does not bond well to SiO_2 or to polymers that are being explored for interlayer dielectric applications. This adhesion problem is particularly serious when subject to thermal cycling. The lack of self-passivation makes Cu thin films susceptible to oxidation during processing (9). Cu interacts with a wide range of materials used in silicon-based devices, including Si, SiO_2, silicides and Al. It is known that Cu diffuses rapidly in Si by an interstitial mechanism and forms deep traps (7). Cu transport in SiO_2 is controlled by both temperature and applied voltage (19). In the presence of an electric field, Cu is observed to drift readily through dielectric films at temperatures as low as 100°C (19, 20). Therefore, among other issues, the challenge of introducing Cu as the new interconnect metal includes blocking the transport of Cu into electrically active regions of devices, and improving the adhesion of Cu to dielectric substrates. The ultimate goal is to find an adhesion promoter between Cu and the interlayer dielectrics that will also perform as a diffusion barrier between Cu and these materials.

1.3. Adhesion Promoters and Diffusion Barriers

Adhesion between two materials can be caused by a physical bonding (van der Waal's forces) or a chemical reaction across the interface. Chemical bonding is the stronger one of the two forces and provides better stability under thermal or mechanical stresses. Cu cannot reduce SiO_2 to adhere strongly to the SiO_2 substrate. Alternative routes have to be taken to enhance the adhesion, such as, using adhesion promoters, increasing deposition temperature and pre-treating the surface with ion implantation or plasma (4-6). Adhesion promoters are effective because they act like a "glue" layer in

between the metal and the dielectric substrate by forming chemical bonds with both layers. This process should be self-limiting, otherwise the integrity of the materials may be compromised with continuous reaction. Thus in effect an ideal adhesion promoter should also behave as a diffusion barrier.

Diffusion barriers are used to prevent undesirable impurities from reaching certain parts of the circuit. In IC applications they are mostly thin layers inserted between metal leads and semiconductor substrates to prevent interdiffusion and chemical reactions. Barriers have been categorized as passive or sacrificial based on the manner in which they work (17). Passive layers are quite inert to the layers on each side and thus, in principle, always keep the two layers separated. Sacrificial barriers will react, at a slow enough or self-limiting rate so that they are still useful. Under this circumstance, barriers serve the dual role of improving adhesion and preventing interactions in the contact area. Therefore the functions of adhesion promoters and diffusion barriers are intertwined. A successful candidate should possess both properties for ULSI application.

In polycrystalline thin films or bulk samples, there are three kinds of defects that contribute to diffusion: vacancies, dislocations and grain boundaries (7). The lattice diffusion occurring by atom-vacancy exchanges is the slowest process, diffusion in dissociated dislocations is intermediate, and grain boundaries (where the misfit between the adjoining lattices is large) have the fastest diffusion rates. Diffusion in polycrystalline thin films is considered to be synonymous with grain boundary diffusion, and the two are used in an interchangeable manner (7). Diffusion in amorphous

materials, on the other hand, depends on their free volume content, owing to the absence of vacancies, dislocations and of course, grain boundaries (7).

A large volume of research has been carried out to determine the applicability of various metals or metallic systems as diffusion barriers/adhesion promoters (7, 11, 19-48). Selection of such a material starts with an investigation of the mutual diffusivity and interaction. Because the diffusivity is directly related to the melting point of the host material, the best diffusion barriers have the highest melting points, e.g., refractory metals (4, 5, 9, 36).

A variety of pure transition metals have been investigated for barrier effects in Cu/M/Si multilayers (M = transition metal) (25, 27, 32, 33, 38, 39, 45). The difference in the barrier properties can be related to the metal-Cu binary phase diagrams and their self-diffusion coefficients (39). An investigation of the binary Cu-metal phase diagrams reveals that many refractory metals, including Ta, W, Mo and V, form virtually no solid solutions with Cu, while Cr, Ti, and Nb form one or more binary phases at low temperatures (9, 36). The formation of Cu-metal binary compounds could result in Cu diffusion through the barrier to the substrate, leading to the silicidation of Cu. The diffusion coefficients of Cu and Si through any barrier layer are of practical importance. The order of self-diffusion coefficients in the transition metals at 400-600ºC is roughly Ti>Cr>Nb>Mo>Ta>W. This trend coincides well with the fact that Ta and W exhibit better diffusion barrier effects against compared to Ti, Cr, Nb and Mo (39).

One method that has been used to improve barrier effectiveness is to intentionally "contaminate" the barrier with impurity atoms (O, N, C, etc.). It is believed that a small

amount of impurites, with limited solubility in the host barrier lattice, will segregate to the grain boundaries and defects, blocking these fast diffusion paths (23, 40, 43, 46). The stability of the barriers can be further extended by amorphous systems. Incorporation of CeO_2 or insertion of a Zr layer into a Ta film significantly improved the diffusion barrier performance by forming an amorphous microstructure (31, 47, 48). Amorphous ternary alloys like M-Si-N (M = Mo, Ta, W) have been reported to prevent Cu diffusion even at 800-900ºC owing to their chemically inert bonds and the elimination of grain boundaries (29, 30, 35, 41, 42).

Although compounding of metals results in better barrier behavior, it may be associated with undesired increase in resistance, counter-balancing the benefit of using Cu to replace Al. A simple computation of the total interconnect resistance suggests the need of a TiN barrier less than 100 Å if we want to take advantage of the resistivity of Cu over that of Al system (49).

1.4. Low-Dielectric-Constant Materials

The replacement of Al by Cu will only reduce the RC delay by approximately 35% (14). Replacement of SiO_2, which has a dielectric constant of up to 4.2, with a low-dielectric-constant material is required for the interconnect structure to reduce propagation delays, cross-talk noise between metal wires, and power dissipation from RC coupling (4, 15, 16, 92).

Interconnect capacitance has two components: the metal line-to-ground and line-to-line. For ULSI designs at 0.25 micron and beyond, line-to-line capacitance plays a dominant role as shown in Figure 1.3 (8). When the width/spacing is scaled down below

0.3 micron, the interlayer capacitance is so small that the total capacitance is dictated by the line-to-line capacitance, which constitutes more than 90% of the total interconnect capacitance. This result highlights the importance of reducing the line-to-line capacitance for sub-quarter-micron devices. Since the capacitance is proportional to the dielectric constant, the replacement of SiO_2 as an intermetal dielectric (IMD) with an insulator with lower dielectric constant is critical to the improvement of device performance.

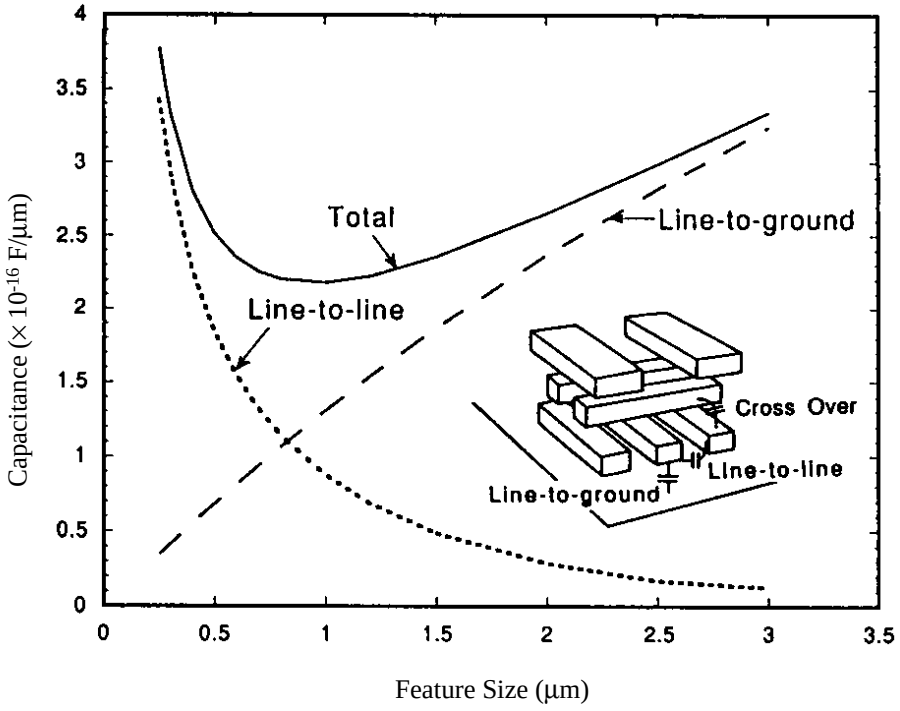

Figure 1.3. Interconnect capacitance as a function of feature size

The dielectric constant (κ) is also known as the relative permittivity (ε_r) because it is referenced to that of free space (vacuum) as shown in Equation (1-2)

$$\kappa = \varepsilon_r = \frac{\varepsilon}{\varepsilon_0} = \frac{\varepsilon_0(1 + \chi_e)}{\varepsilon_0} = 1 + \chi_e \qquad (1\text{-}2)$$

where ε and ε_0 are the permittivity (F/m) of the dielectric and free space respectively, and χ_e is the electric susceptibility of the dielectric material.

In general, ε_r is a complex number. Its imaginary term may usually be neglected, except at very high frequencies (50). The real component of ε_r is often called the dielectric constant (κ). Its value depends on frequency, temperature and other factors (50). Because of its simple numeric expression, as compared to the absolute permittivity (ε), κ is generally used to describe the dielectric property of materials in IC applications. In many publications, the symbol ε is conventionally used in place of κ to refer to the dielectric constant and the expression of "low-*k*" or "low k" is used to refer to the low-dielectric-constant materials.

The dielectric constant is a physical measure of the electric polarizability of a material. It describes the tendency of a material to permit an applied electric field to induce dipoles in the material. χ_e is related to the electric polarization (P) and the applied electric field (E) in

$$P = \varepsilon_0 \chi_e E \qquad (1\text{-}3)$$

P is the total dipole moment induced in a unit volume of the dielectric (C/m^2) and E is the field strength (V/m).

The magnitude of the dielectric constant is dependent upon the ability of the polarizable units in the material to orient fast enough to keep up with the oscillations of an alternating electric field. The polarization mechanisms which comprise the dielectric constant can be electronic, atomic and dipolar (51). At optical frequencies (10^{14} Hz), only the lowest mass species, electron, are efficiently polarized. At lower frequencies, atomic polarization of heavier, more slowly moving nuclei also contribute to the dielectric constant. Atomic polarization occurs in the infrared (10^{12} Hz) or lower frequency regimes. Dipole polarization is the redistribution of charge when a group of atoms with a permanent dipole align in response to the electric field. In the solid state, alignment of permanent dipoles requires considerably more time than electronic or atomic polarization, therefore it happens at microwave (10^9 Hz) or lower frequencies (51). The contribution of each polarization mode to the dielectric constant is generally additive, i.e.

$$\kappa = \kappa_{electronic} + \kappa_{atomic} + \kappa_{dipolar} \qquad (1\text{-}4)$$

Strategies for lowering the dielectric constant include minimizing polarizability, maximizing free volume and fluorination (51). Materials with few polar function groups are commonly chosen for the first purpose. The introduction of free volume decreases the number of polarizable groups per unit volume, resulting in lower values for κ_{atomic} and $\kappa_{dipolar}$. The addition of pendant groups, flexible bridging units, and bulky groups which limit chain packing density have all been used to enhance free volume in polymers (51).

Fluorine substitution reduces κ by a combination of lower polarizability and moisture absorption and larger free volume. Substitution –H with –F or $–CF_3$ groups decreases the electronic polarizability due to strong electron-withdrawing inductive effects. The bulky $–CF_3$ group can reduce efficient molecular packing and increase the free volume. The hydrophobicity introduced by F substitution is important since moisture, even in small concentrations, strongly affects the dielectric constant due to the large κ value of water (78.5 at 25°C) (52).

Strong efforts are being invested to find a suitable insulator material with a dielectric constant below 3.0 (14, 19-21, 34, 52-91). Recent developments in this area are the subject of several review articles (4, 15, 16, 92) as well as the symposium proceedings of Materials Research Society (MRS) (73, 93-95) and MRS Bulletin (96). Under Sematech's sponsorship, a cross section of industrial representatives have determined a list of requirements for the new low k dielectric materials (53). They are listed in Table 1.3.

At this time, the industry has not compiled a standard for low k materials properties. The requirements may vary from one application to another and depend on the interconnect architecture (14).

Table 1.3. Requirements for low dielectric constant ILD materials

Electrical	Chemical	Mechanical	Thermal
Anisotropy	Chemical resistance	Thickness uniformity	High thermal stability
Low dissipation	Etch selectivity	Good adhesion	Low coefficient of thermal expansion
Low leakage current	Low moisture absorption	Low stress	Low thermal shrinkage
Low charge trapping	Low solubility in water	High hardness	Low thermal weight loss
High electric-field strength	Low gas permeability	Low shrinkage	High thermal conductivity
High reliability	High purity	Crack resistance	
	No metal corrosion	High tensile modulus	
	Long storage life		
	Environmentally safe		

There are a wide variety of dielectric materials with κ values less than that of SiO_2. These materials, as listed in Table 1.4 (53, 96, 97), can be either organic or inorganic and they can be deposited by either spin-on or chemical vapor deposition (CVD) techniques. Spin-on deposition involves dissolving low k precursors in a solvent, dispensing the liquid mixture onto the wafer, and curing subsequently to drive the solvent out. Polymerization occurs during the curing to form a solvent-resistant dielectric film. Spin-on is a rather simple method. It can be applied to a large variety of precursors. The designs of equipment are also similar for different applications. CVD offers a number of advantages. First, it is a dry process which eliminates the cost and environmental issues associated with organic solvents. Secondly, it provides uniform coating over large areas. This is especially attractive for future 300mm wafers. Lastly, it also has superior gap-filling capability for high aspect-ratio (depth versus width) vias and trenches (74).

Table 1.4. List of materials for ILD applications

Material	Dielectric constant	Deposition method
Inorganic		
SiO_2	3.9-5.0	CVD
Fluorinated SiO_2	2.8-3.9	CVD
Spin-on glasses (SOGs)	2.7-3.5	Spin-on
Organic		
Polyimides	2.9-3.9	Spin-on/CVD
Fluorinated polyimides	2.3-2.8	Spin-on/CVD
Benzocyclobutene (BCB)	2.7	Spin-on
Parylenes (N and F)	2.3-2.7	CVD
Polynaphthalene	2.3	CVD
Fluorinated amorphous carbon (a-C:F)	2.1-2.3	CVD
Amorphous Teflon	1.9	Spin-on
Inorganic-organic hybrids	2.8-3.0	Spin-on
Nanoporous dielectrics	1.2-1.8	Spin-on
Air bridge	1.0-1.2	

Dielectric constant values vary from different references. Ranges are chosen to include all possible values.

The integration of low k materials is intimately related to optimizing different trade-offs between material properties, device architectures and process flows. The high processing temperature (~400°C), which involves both Al metallization and plasma damage sintering, has led to the primary focus on thermally stable inorganic materials. Low k inorganic polymers are usually based on siloxane chemistry and have an O-Si-O backbone. Hydrogen silsesquioxane (HSQ), in which the silicon atoms are directly

attached to oxygen and hydrogen, is stable to 400°C and has a dielectric constant of 2.9. Increasing the carbon content in siloxanes tends to lower the dielectric constant as well as increase the thermal stability of the film because of the substitution of Si-H bonds with stronger Si-C bonds. Methyl silsesquioxane (MSQ) have a methyl group on every Si atom and a similar ladder structure to HSQ. It has a dielectric constant of 2.7, which is stable when exposed to air for months. It also has very high thermal stability (>500°C in the absence of air) and good resistance to stress and cracking (66). The rapid development of Cu metallization will allow deposition temperatures as low as 100°C, which may finally permit the integration of organic materials as long as parallel reductions in the plasma damage sinter temperature are developed.

Since the lowest dielectric constant for any dense material is approximately 2.0 for Teflon, the evaluation of nanoporous dielectrics will eventually be required to push performance to its fundamental limits. For a porous material, the dielectric constant is a combination of that of air (~1) and the solid phase. The ultra-low dielectric constant results from porosity incorporation. These porous materials are classified as aerogels (dried supercritically) or xerogels (dried by solvent evaporation) (68). In addition to low k, nanoporous material offers other advantages such as thermal stability to 900°C, tunable film density over a wide range, and ability to use the same material, equipment and integration scheme for multiple technology nodes. The problem is how to achieve high strength and porosity yet maintain pores much smaller than microelectronic features.

The major driving forces for determining the future of low k material integration are dielectric constant, process cost, and process reliability. The ultimate solution will be determined by the best compromise among these three factors (71).

1.5. Experimental Aspects

Processes occurring at solid surfaces are of great importance particularly for the studies of heterogeneous catalysis, corrosion and semiconductor technology. A surface can be visualized as the result of a fracture along a certain plane in the bulk material, where the bonds between neighboring atoms are simply severed. The change in the equilibrium position and bonding of surface atoms can give rise to drastic reconstruction of the outermost layers, i.e., the surface can assume a fundamentally different atomic structure from that of the bulk material (98-101). The surface has a strong tendency to interact chemically with particles from the gas phase because of the more or less unsaturated valencies. In order to maintain the original state for long enough to conduct experiments, it is clearly necessary to keep the pressure of the residual gas above the surface very low, which calls upon the ultra high vacuum (UHV) techniques.

The concentration of atoms on the surface of a solid is on the order of 10^{15} cm^{-2}. A rough calculation reveals that at a pressure of 10^{-6} torr, the surface will be covered with a monolayer of gas within a second at room temperature if the sticking coefficient is 1. For this reason the unit of gas exposure is 10^{-6} torr-sec, which is called a langmuir (L) (99). Current surface techniques can easily detect contamination on the order of 1% of a monolayer. This gives the operational definition of a “clean” surface. Thus, pressures lower than 10^{-9} torr (so-called ultra high vacuum (UHV) conditions), are necessary to

maintain a clean surface for about one hour, often the time scale needed to perform one experiment (99, 101).

Several UHV-based surface analytical methods were employed in this research, including Auger electron spectroscopy (AES) and temperature programmed desorption (TPD). The principles of operation for each technique are discussed as follows.

1.5.1 Auger Electron Spectroscopy (AES).

Auger electron spectroscopy is suitable for studying the composition of surfaces. It can probe the first few layers of the surface by measuring the kinetic energy of emitted electrons. The surface sensitivity of AES is due to the low energy of these electrons ($E \leq 1000$ eV). Electrons in this energy range interact with solid matter very strongly, therefore their mean free path within the solid is consequently only a few atomic layers , making this an ideal tool for surface analysis (99-101).

The Auger process involves three electrons as shown in Figure 1.4 (99). When an electron beam strikes the atoms of a material, a core level (K) electron can be ejected if the incident beam energy is greater than the binding energy of the electrons in level K (E_K). Following the excitation that creates a hole in level K, the atom relaxes by filling the hole via a transition from an outer level, in this example L_1. The energy released from this transition may cause a third electron either in the same or a higher lying level (L_3 in this example) to emit into the vacuum. The third electron is called an Auger electron. The Auger transition in this particular example is labeled conventionally as KL_1L_3. If we ignore the Coulombic interaction between the two holes in the final state

(since in metals and semiconductors, the final state holes are well screened from each other (102)), the kinetic energy of this Auger electron is approximated by:

$$E_{K L_1 L_3} = E_K - E_{L_1} - E_{L_3} \quad (1\text{-}5)$$

The Auger energy is a function only of the different atomic energy levels. Since there are no two elements with the same set of atomic binding energies, the analysis of Auger energies leads to elemental identification. In selected cases, chemical binding information can also be obtained from peak position, shape or fine structures. Because Auger peak-to-peak intensity is proportional to the amount of atoms on the surface, AES studies can be quantitative as well as qualitative.

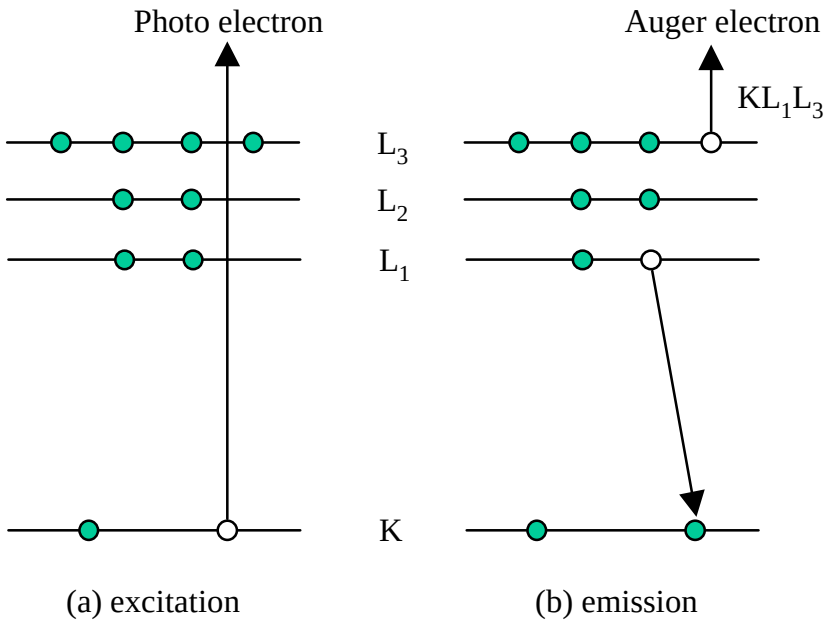

Figure 1.4. Scheme of the Auger emission process

The integrated Auger spectra (N(E) vs. E) are less useful because Auger features have a large secondary emission background as shown in Figure 1.5(a). Auger spectra are therefore often recorded as the differential with respect to energy as in Figure 1.5(b) (100). It can be seen that differentiation helps to remove the background and make weak features more identifiable.

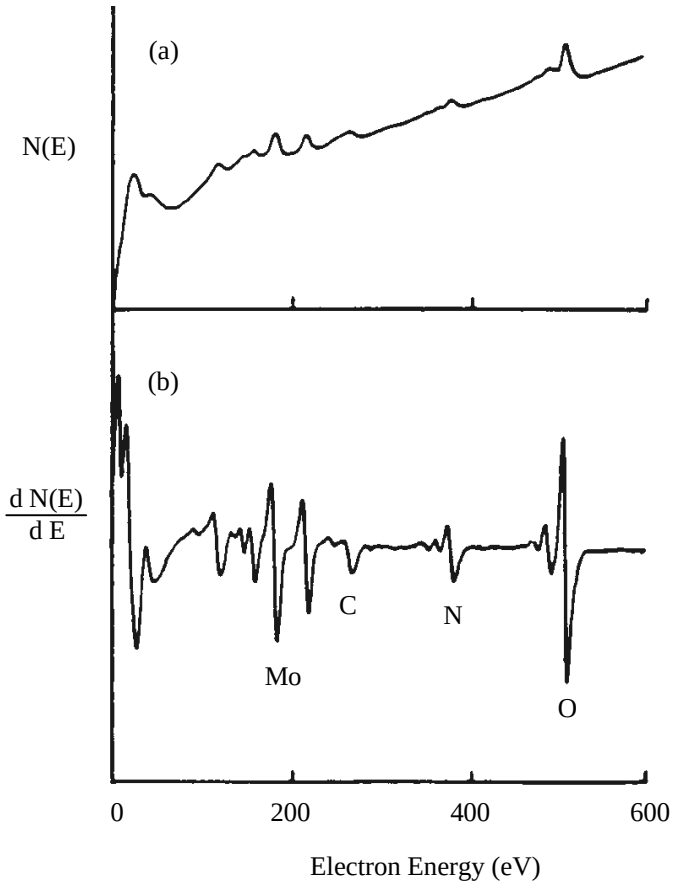

Figure 1.5. Auger spectra from a contaminated molybdenum surface in (a) integrated and (b) differentiated modes.

1.5.2. Temperature Programmed Desorption (TPD)

Temperature programmed desorption is a technique for studying surface reactions and molecular adsorption on surfaces (99, 103, 104). Figure 1.6 shows the schematic diagram of TPD. The basic operation involves, first, adsorption of molecular species onto the sample surface at low temperature, then, heating of sample in a controlled manner (usually at a rate β which is linear to time) while monitoring the evolution of species from the surface back into the gas phase. The detector is generally a quadrupole mass spectrometer (QMA) and is placed as close as possible to the sample so as to exclude outgassing species from other than the sample surface and get maximum signal detection. The whole process is generally carried out under computer control with quasi-simultaneous recording of a large number of possible products. The data obtained from such an experiment consists of the intensity variation of each recorded mass fragment as a function of temperature and is called a TPD spectrum (103).

Since the molecular species initially adsorbed on the surface can undergo reaction pathways with different activation parameters, such as dissociation, recombination and compound formation with substrate, the analysis of TPD spectra provides kinetic information and possible mechanism of the surface reaction. During the study of a specific system, TPD spectra are generally taken for a serial of different initial coverages. The area under a peak is proportional to the amount of the adsorbate. The peak profile and the coverage dependence of the desorption characteristics give information on the aggregation state of the adsorbed species (i.e., associative or dissociative). The position of the peak, which is the temperature where maximum desorption occurs, is related to the

enthalpy of adsorption and thereby, is related to the binding strength to the surface. That is why if there is more than one binding state for an adsorbate species on a surface with significantly different adsorption enthalpies, it will give rise to multiple peaks in the TPD spectrum (99, 103, 104).

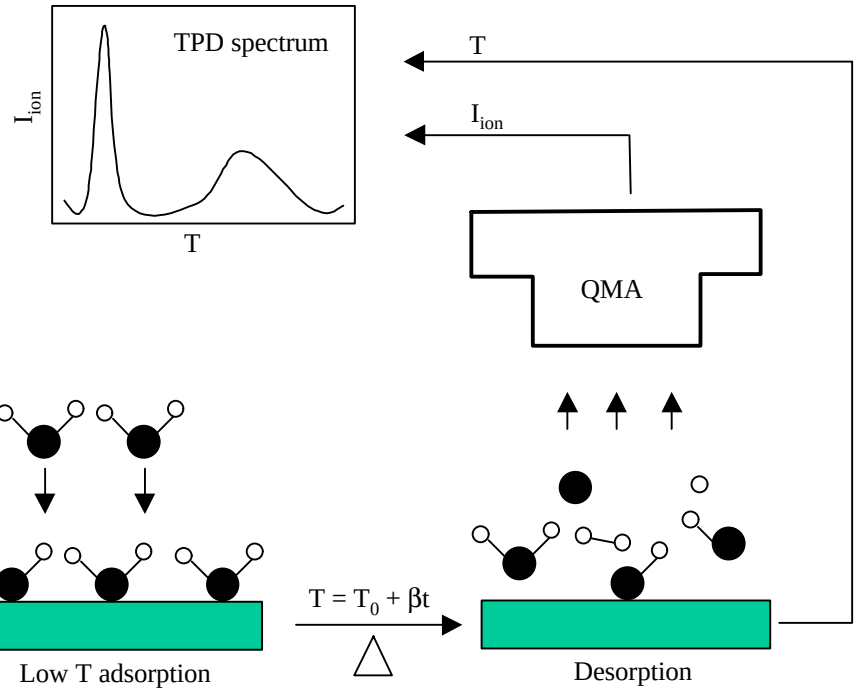

Figure 1.6. Scheme of the TPD process

1.6. Chapter References

(1) *The National Technology Roadmap for Semiconductors: Technology Needs*; Semiconductor Industry Association: San Jose, CA, 1997.

(2) Runyan, W. R.; Bean, K. E. In *Semiconductor Integrated Circuit Processing Technology*; Addison-Wesley Publishing Company: Reading, MA, 1990, pp 124-126.

(3) Singer, P. *Semiconductor International* **1997,** *Nov.*, 67.

(4) Murarka, S. P. *Mater. Sci. Eng.* **1997,** *R19*, 87-151.

(5) Murarka, S. P.; Hymes, S. W. *Crit. Rev. Solid State Mater. Sci.* **1995,** *20*, 87-124.

(6) Murarka, S. P.; Gutmann, R. J.; Kaloyeros, A. E.; Lanford, W. A. *Thin Solid Films* **1993,** *236*, 257-266.

(7) Gupta, D. *Mater. Chem. Phys.* **1995,** *41*, 199-205.

(8) Jeng, S.-P.; Havemann, R. H.; Chang, M.-C. *Mat. Res. Soc. Symp. Proc* **1994,** *337*, 25.

(9) Li, J.; Shacham-Diamond, Y.; Mayer, J. W. *Mater. Sci. Rep.* **1992,** *9*, 1-51.

(10) Lanford, W. A.; Ding, P. J.; Wang, W.; Hymes, S.; Murarka, S. P. *Mater. Chem. Phys.* **1995,** *41*, 192-198.

(11) Torres, J.; Mermer, J. L.; Madar, R.; Crean, G.; Gessner, T.; Bertz, A.; Hasse, W.; Plotner, M.; Binder, F.; Save, D. *Microelctronic Eng.* **1996,** *34*, 119-122.

(12) Shacham-Diamond, Y.; Dubin, V. M. *Microelectronic. Eng.* **1997,** *33*, 47-58.

(13) Modified from "http://www.chips.ibm.com/gallery/p-cw2.html".

(14) Lee, W. W.; Ho, P. S. *MRS Bull.* **1997,** *22*, 19.

(15) Treichel, H.; Ruhl, G.; Ansmann, P.; Wurl, R.; Muller, c.; Dietlmeier, M. *Microelectronic Eng.* **1998,** *40*, 1-19.

(16) Murarka, S. P. *Solid State Technol.* **1996,** *39*, 83.

(17) Runyan, W. R.; Bean, K. E. In *Semiconductor Integrated Circuit Processing Technology*; Addison-Wesley Publishing Company: Reading, MA, 1990, pp 518-578.

(18) McBrayer, J. D.; Swanson, R. M.; Sigmon, T. W. *J. Electrochem. Soc.* **1986,** *133*, 1242.

(19) Raghavan, G.; Chiang, C.; Anders, P. B.; Tzeng, S.-M.; Villasol, R.; Bai, G.; Bohr, M.; Fraser, D. B. *Thin Solid Films* **1995,** *262*, 168.

(20) Loke, A. L. S.; Ryu, C.; Yue, C. P.; Cho, J. S. H.; Wong, S. S. *IEEE Electron Device Lett.* **1996,** *17*, 549.

(21) Chang, C.-A.; Yee, D. S.; Petkie, R. *Appl. Phys. Lett.* **1989,** *54*, 2545.

(22) Chang, K.-M.; Yeh, T.-H.; Deng, I.-C.; Shih, C.-W. *J. Appl. Phys.* **1997,** *82*, 1469.

(23) Clevenger, L. A.; Bojarczuk, N. A.; Holloway, K.; Harper, J. M. E.; C Cabral, J.; Schad, R. G.; Cardone, F.; Stolt, L. *J. Appl. Phys.* **1993,** *73*, 300.

(24) Holloway, K.; fryer, P. M.; Jr, C. C.; Harper, J. M. E.; Bailey, P. J.; Kelleher, K. H. *J. Appl. Phys.* **1992,** *71*, 5433.

(25) Hu, C.-K.; Chang, S.; Small, M. B.; Lewis, J. E. *Proceedings of the International VLSI Multilevel Interconnection Conference* **1986**, 181-187.

(26) Imahori, J.; Oku, T.; Murakami, M. *Thin Solid Films* **1997,** *301*, 142-148.

(27) Jang, S.-Y.; Lee, S.-M.; Baik, H.-K. *J. Mater. Sci.: Mater. Electronics* **1996,** *7*, 271-278.

(28) Kaloyeros, A. E.; Chen, X.; Stark, T.; Kumar, K.; Seo, S.; Peterson, G. G.; Frisch, H. L.; Arkles, B.; Sullivan, J. *J Electrochem. Soc* **1999,** *146*, 170-176.

(29) Kim, D. J.; Kim, Y. T.; Park, J.-W. *J. Appl. Phys.* **1997,** *82*, 4847.

(30) Kolawa, E.; Pokela, P. J.; Reid, J. S.; Chen, J. S.; Nicolet, M.-A. *Appl. Surf. Sci.* **1991,** *53*, 373-376.

(31) Kwak, J. S.; Baik, H. K.; Kim, J.-H.; Lee, S.-M. *Appl. Phys. Lett.* **1998,** *72*, 2832.

(32) Kwon, K.-W.; Ryu, C.; Sinclair, R.; Wong, S. S. *Appl. Phys. Lett.* **1997,** *71*, 3069.

(33) Kwon, K.-W.; Lee, H.-J.; Ryu, C.; Sinclair, R.; Wong, S. S. *Advanced Metallization and Interconnect Systems for ULSI Applications; Conference Proceedings* **1997**, 711-716.

(34) Lacerda, M. M.; Jr, F. L. F.; Esteves, J. H. C. R.; Achete, C. A. *J. Phys. D: Appl. Phys.* **1997,** *30*, 944.

(35) Lee, Y.-J.; Suh, B.-S.; Kwon, M. S.; Park, C.-O. *J. Appl. Phys.* **1999,** *85*, 1927.

(36) Li, J.; Strane, J. W.; Russell, S. W.; Hong, S. Q.; Mayer, J. W.; Marais, T. K.; Theron, C. C.; Pretorius, R. *J. Appl. Phys.* **1992,** *72,* 2810.

(37) Lin, J.-C.; Lee, C. *Electrochem. Solid-State Lett.* **1999,** *2,* 181-183.

(38) Olowolafe, J. O.; Mogab, C. J.; Gregory, R. B. *Thin Solid Films* **1993,** *227,* 37-43.

(39) Ono, H.; Nakano, T.; Ohta, T. *Appl. Phys. Lett.* **1994,** *64,* 1511.

(40) Ono, H.; Nakano, T.; Ohta, T. *Jpn. J. Appl. Phys. Part 1* **1995,** *34,* 1827-1830.

(41) Reid, J. S.; Kolawa, E.; Ruiz, R. P.; Nicolet, M.-A. *Thin Solid Films* **1993,** *236,* 319-324.

(42) Reid, J. S.; Lin, R. Y.; Smith, P. M.; Ruiz, R. P.; Nicolet, M.-A. *Thin Solid Films* **1995,** *262,* 218.

(43) Stavrev, M.; Fischer, D.; Preub, A.; Wenzel, C.; Mattern, N. *Microelectronic Eng.* **1997,** *33,* 269-275.

(44) Wang, M. T.; Lin, Y. C.; Chen, M. C. *J. Electrochem. Soc.* **1998,** *145,* 2538.

(45) Wong, S. S.; Ryu, C.; Lee, H.; Kwon, K.-W. *Mater. Res. Soc. Symp. Proc.* **1998,** *514,* 75.

(46) Wang, W.; Booske, J. H.; Liu, H. L.; Gearhart, S. S.; Shohet, J. L.; Bedell, S.; Lanford, W. *J. Mater. Res.* **1998,** *13,* 726.

(47) Yoon, D.-S.; Baik, H. K.; Lee, S.-M. *J. Appl. Phys.* **1998,** *83,* 8074.

(48) Yoon, D.-S.; Baik, H. K.; Lee, S.-M. *J. Vac. Sci. Technol. B* **1999,** *17,* 174.

(49) Berti, A.; Murarka, S. P. *Mater. Res. Soc. Symp. Proc.* **1994,** *318,* 451.

(50) Fink, D. G.; McKenzie, A. A. *Electronics Engineers' Handbook*; 1st Ed.; McGraw-Hill Book Company, 1975.

(51) Simpson, J. O.; Clair, A. K. S. *Thin Solid Films* **1997,** *308-309,* 480-485.

(52) Ryan, E. T.; McKerrow, A. J.; Leu, J.; Ho, P. S. *MRS Bull.* **1997,** *22,* 49.

(53) Ting, C. H.; Seidel, T. E. *Mat. Res. Soc. Symp. Proc.* **1995,** *381,* 3.

(54) Du, M.; Opila, R. L.; Donnelly, V. M.; Sapjeta, J.; Boone, T. *J Appl. Phys.* **1999,** *85*, 1496.

(55) Du, M.; Opila, R. L.; Case, C. *J. Vac. Sci. Technol. A* **1998,** *16*, 155.

(56) Endo, K.; Tatsumi, T. *J. Appl. Phys.* **1995,** *78*, 1370.

(57) Endo, K.; Tatsumi, T. *Mat. Res. Soc. Symp. Proc.* **1995,** *381*, 249.

(58) Endo, K.; Tatsumi, T. *Appl. Phys. Lett.* **1996,** *68*, 2864.

(59) Endo, K.; Tatsumi, T. *Appl. Phys. Lett.* **1996,** *68*, 3656.

(60) Endo, K.; Tatsumi, T.; Matsubara, Y. *Jpn. J. Appl. Phys.* **1996,** *35*, L 1348.

(61) Endo, K.; Tatsumi, T. *Appl. Phys. Lett.* **1997,** *79*, 2616.

(62) Endo, K. *MRS Bull.* **1997,** *22*, 55.

(63) Gaynor, J.; Ralston, A. *Semiconductor International* **1997,** *Dec.*, 73.

(64) Grill, A.; Patel, V. *J. Appl. Phys.* **1999,** *85*, 3314.

(65) Gutmann, R. J.; Chow, T. R.; Lakshminarayanan, S.; Price, D. T.; Steigerwald, J. M.; You, L.; Murarka, S. P. *Thin Solid Films* **1995,** *270*, 472-479.

(66) Hacker, N. P. *MRS Bull.* **1997,** *22*, 33.

(67) Han, L. M.; Timmons, R. B.; Lee, W. W.; Chen, Y.; Hu, Z. *J. Appl. Phys.* **1998,** *84*, 439.

(68) Jin, C.; Luttmer, J. D.; Smith, D. M.; Ramos, T. A. *MRS Bull.* **1997,** *22*, 39.

(69) Kudo, H.; Shinohara, R.; Yamada, M. *Mat. Res. Soc. Symp. Proc.* **1995,** *381*, 105.

(70) Limb, S. J.; Labelle, C. B.; Gleason, K. K.; Edell, D. J.; Gleason, E. F. *Appl. Phys. Lett.* **1996,** *68*, 2810.

(71) List, R. S.; Singh, A.; Ralston, A.; Dixit, G. *MRS Bull.* **1997,** *22*, 61.

(72) Liu, P. T.; Chang, T. C.; Sze, S. M.; Pan, F. M.; Mei, Y. J.; Wu, W. F.; Tsai, M. S.; Dai, B. T.; Chang, C. Y.; Shih, F. Y.; Huang, H. D. *Thin Solid Films* **1998,** *332*, 345-350.

(73) Lu, T.-M.; Murarka, S. P.; Kuan, T.-S.; Ting, C. H. ; Mater. Res. Soc. Symp. Proc., 1995; Vol. 381.

(74) Lu, T.-M.; Moore, J. A. *MRS Bull.* **1997,** *22*, 28.

(75) Ma, Y.; Yang, H.; Guo, J.; Sathe, C.; Agui, A.; Nordgren, J. *Appl. Phys. Lett.* **1998,** *72*, 3353.

(76) Miller, R. D.; Hedrick, J. L.; Yoon, D. Y.; Cook, R. F.; Hummel, J. P. *MRS Bull.* **1997,** *22*, 44.

(77) Mountsier, T. W.; Kumar, D. *Mat. Res. Soc. Symp. Proc.* **1997,** *443*, 41.

(78) Muller, U.; Oral, R. H.; Tobler, M. *Surf. Coat. Technol.* **1995,** *76-77*, 367-371.

(79) Park, J. M.; Matienzo, L. J.; Spencer, D. F. *J. Adhersion Sci. Technol.* **1991,** *5*, 153.

(80) Sacher, E. *Prog. Surf. Sci.* **1994,** *4*, 273.

(81) Senkevich, J. J.; Desu, S. B. *Appl. Phys. Lett* **1998,** *72*, 258.

(82) Singer, P. *Semiconductor International* **1998**, 42.

(83) Sullivan, J. P.; Denison, D. R.; Barbour, J. C.; Newcomer, P. P.; Apblett, C. A.; Seager, C. H.; Baca, A. G. *Mat. Res. Soc. Symp. Proc.* **1997,** *443*, 149.

(84) Sutcliffe, R.; Lee, W. W.; Gaynor, J. F.; Luttmer, J. D.; Martini, D.; Kelber, J.; Plano, M. A. *Appl. Surf. Sci.* **1998,** *126*, 43.

(85) Theil, J. A.; Mertz, F.; Yairi, M.; Seaward, K.; Ray, G.; Kooi, G. *Mat. Res. Soc. Symp. Proc.* **1997,** *476*, 31.

(86) Vogt, M.; Kachel, M.; Melzer, K.; Drescher, K. *Surf. Coat. Technol.* **1998,** *98*, 948.

(87) Yang, H.; Tweet, D. J.; Ma, Y.; Nguyen, T. *Appl. Phys. Lett* **1998,** *73*, 1514.

(88) Yokomichi, H.; Hayashi, T. *Appl. Phys. Lett.* **1998,** *72*, 2704.

(89) Yokomichi, H.; Hayashi, T.; Amano, T.; Masuda, A. *J. Non-Cryst. Solids* **1998,** *227-230*, 641.

(90) Yun, S.-M.; Chang, H.-Y.; Kang, M.-S.; Choi, C.-K. *Thin Solid Films* **1999,** *341*, 109-111.

(91) Zhao, B.; Feiler, D.; Ramanathan, V.; Liu, Q. Z.; Brongo, M.; Wu, J.; Zhang, H.; Kuei, J. C.; Young, D.; Brown, J.; Vo, C.; Xia, W.; Chu, C.; Zhou, J.; Nguyen, C.; Tsau, L.; Dornisch, D.; Camilletti, L.; Ding, P.; Lai, G.; Chin, B.; Krishna, N.; Johnson, M.; Turner, J.; Ritzdorf, T.; Wu, G.; Cook, L. *Electrochem. Solid-State Lett.* **1998,** *1*, 276-278.

(92) Homma, T. *Mater. Sci. Eng.* **1998,** *R23*, 243-285.

(93) Chiang, C.; Ho, P. S.; Lu, T.-M.; Wetzel, J. T. ; Mater. Res. Soc. Symp. Proc., 1998; Vol. 511.

(94) Case, C.; Kohl, P.; Kikkawa, T.; Lee, W. W. ; Mater. Res. Soc. Symp. Proc., 1997; Vol. 476.

(95) Lagendijk, A.; Treichel, H.; Uram, K. J.; Jones, A. C. ; Mater. Res. Soc. Symp. Proc., 1996; Vol. 443.

(96) *MRS Bull.* **1997,** *22*.

(97) Jeng, S.-P.; Taylor, K.; Chang, M.-C.; Ting, L.; Lee, C.; McAnally, P.; Seha, T.; Numata, K.; Tanaka, T.; Havemann, R. H. *Mat. Res. Soc. Symp. Proc.* **1995,** *381*, 197.

(98) Somorjai, G. A. *MRS Bull.* **1998,** *23*, 11.

(99) Somorjai, G. A. *Introduction to Surface Chemistry and Catalysis*; John Wiley & Sons, Inc., 1994.

(100) Briggs, D.; Seah, M. P. In *Practical Surface Analysis*; John Wiley & Sons Ltd, 1990; Vol. 1.

(101) Ertl, G.; Kuppers, J. *Low Energy Electrons and Surface Chemistry*; VCH Publishers: New York, 1985.

(102) Jennison, D. R.; Kelber, J. A.; Rye, R. R. *Phys. Rev. B* **1982,** *25*, 1384.

(103) Nix, R. *An Introduction to Surface Science*; http.//www.chem.qmw.ac.uk/surfaces/scc/sccinfo.htm, 1997.

(104) Redhead, P. A. *Vacuum* **1962,** *12*, 203.

CHAPTER 2

FORMATION OF POLYMERIC CARBON-SILICON FILMS ON METAL SUBSTRATES: ADHESION/DIFFUSION BARRIERS FOR COPPER

2.1. Introduction

The introduction of Cu in multilevel metallization architectures has spurred the demand for more effective diffusion barriers (1). Refractory metals and their compounds have been extensively investigated in this regard (2-7). Additionally, the possible replacement of SiO_2 with low-dielectric polymeric materials has raised issues regarding the adhesion of the polymer to Cu or other metal substrates, and the diffusion of Cu into the polymer (8-12).

Organosilicon compounds have been used to modify surfaces by self-assembly (13-17). Such compounds are referred to as silane coupling agents (SCAs) because they act as a bridge between organic and inorganic phases. The general formula for these silanes is $RSiX_3$, where R is an organic group and X is a hydrolyzable group, typically alkoxy or chloride. The binding mechanism of silanes to the surface consists of a complex series of hydrolysis and condensation reactions, resulting in a cross-linked network of siloxanes that are covalently bound to the surface (15). The self-assembly method typically involves immersing the sample in a solution that contains the silanes, followed by rinsing and drying. The final structure of the siloxane varies greatly depending on the functionality of the silane and the experimental conditions.

This chapter presents the studies of the formation of polymeric carbon-silicon (C-Si) films via electron-beam or ultra-violet (UV) radiation induced polymerization of vinyl-silane derivative precursors. The research was carried out under ultra high vacuum (UHV) conditions. Introduction of the silane precursors was through vapor phase adsorption, which completely eliminated the effect of solvents. Such films are referred to as "C-Si" rather than SiC (silicon carbide) because the compositions of the films appear quite close to that of the precursors: vinyltrichlorosilane ($H_2C=CHSiCl_3$, VTCS) or vinyltrimethylsilane ($H_2C=CHSi(CH_3)_3$, VTMS). The films thus formed are compositionally quite different from the SiC films formed by, e.g., e-beam induced reaction of methyl silane (18), and therefore might be expected to display different mechanical, chemical and electronic properties. Furthermore, the close correspondence between the film composition and that of the precursor indicates that films with molecularly tailored properties can be formed by a systematic variation in precursor chemistry. The potential application of these films is twofold, as demonstrated in Figure 2.1. First, the C_x-Si film formed by vinyl-silane precursors alone can act as diffusion barrier for Cu. Secondly, it can be used as an anchor layer for fluoropolymers by introducing F-containing precursors in the polymerization process. Fluoropolymers are an important candidate for low dielectric materials but their adhesion properties are weak (9, 11, 19, 20). Films generated by this method can provide an adhesive interface between metal and polymers.

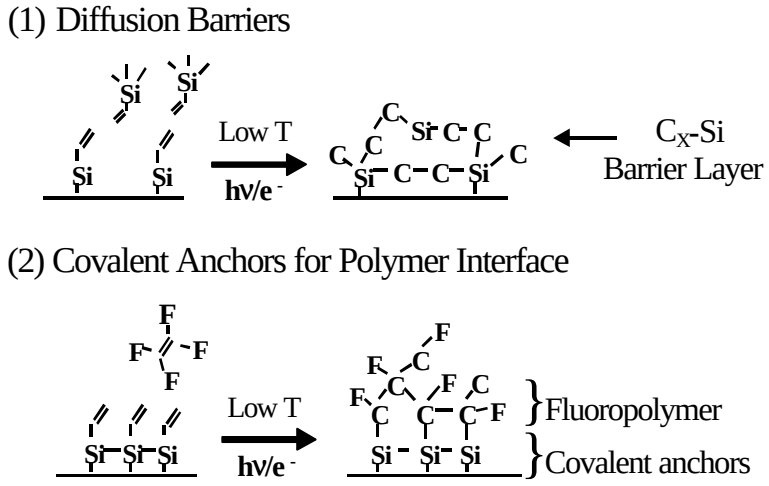

Figure 2.1. Scheme of the potential applications of C-Si films.

Temperature programmed desorption (TPD) and Auger electron spectroscopy (AES) data are presented in this chapter to demonstrate that electron or UV bombardment induced polymerization occurs via the reactions of the vinyl groups of adsorbed precursors, and that film composition parallels precursor composition. AES results indicate that such films are potential candidates for Cu diffusion barriers even at thicknesses of ~ 100 Å. Films derived from VTMS are adherent and stable on Ta substrates until 1000 K with the ability to resist Cu thermal diffusion at above 800 K in UHV. Films polymerized in the presence of adsorbed hexafluorobenzene display the incorporation of fluorobenzene units. The stability of these films toward moisture depends on the structure of the precursors.

2.2. Experimental Methods

Experiments were carried out in a UHV chamber maintained by a turbomolelar pump and an ion/titanium sublimation pump (TSP) (21, 22). The schematic diagram of the chamber is shown in Figure 2.2. Typical working pressures in the chamber were 2-5 x 10^{-10} Torr. The background pressure was monitored by a nude ion gauge calibrated for dinitrogen and located out of line-of-sight to the sample in order to avoid electron-induced surface reactions. The chamber was equipped with a quadrupole mass analyzer (UTI, Model 100c) for both residual gas analysis and TPD studies. In the TPD experiments, the sample was positioned at a distance of less than 5 mm in front of a collimated shroud (10 mm diameter) for line-of-sight measurements. A linear heating rate of ~8 K/s was used in all TPD experiments.

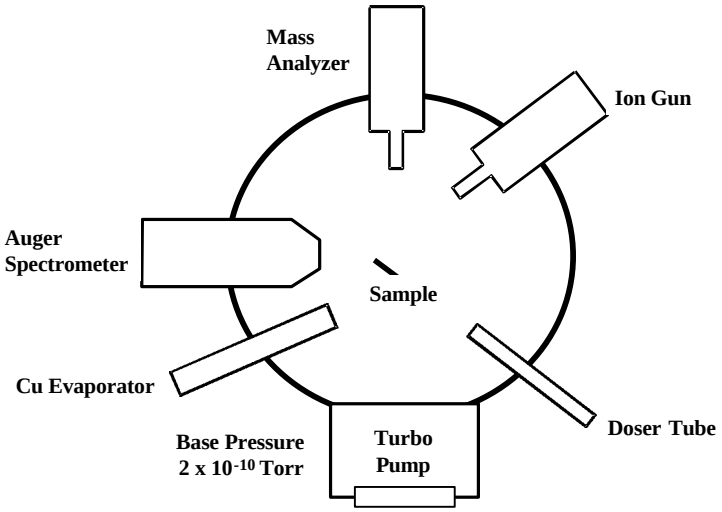

Figure 2.2. Schematic diagram of the UHV chamber used for TPD and AES studies.

The chamber was also equipped with an Auger spectrometer system (Physical Electronics, Model 101-50) using a cylindrical mirror analyzer (CMA) with co-axial electron gun. Auger spectra were collected in the derivative (dN(E)/d(E)) mode using a lock-in amplifier at 4V peak to peak modulation and an XY recorder. The electron excitation energy was 3 KeV. Relative concentrations of surface species were determined by using published (23) Auger sensitivity factors and intensities proportional to peak-to-peak signal height according to

$$N_A/N_B = I_A X_B / I_B X_A \qquad (2\text{-}1)$$

Where N, I and X represent respectively, the atomic concentration, the peak-to-peak intensity and the atomic sensitivity factor of a certain element. The thickness of an overlayer was calculated using the equation

$$I = I_0 \exp(-d/\lambda) \qquad (2\text{-}2)$$

Where I_0 and I are the intensities of substrate signal before and after the overlayer deposition respectively, and d is the thickness of the overlayer, and λ is the inelectric mean free path of the specified transition.

Metal samples of Cu, Al and Ta consisted of polycrystalline foils ~ 1 cm^2 in area and < 0.1 mm thick. The Ta sample was directly attached to the manipulator by two Ta support leads. Due to their low resistivity, Cu and Al samples were mounted to a Ta sample holder and then spot-welded to the Ta leads. The sample temperature was monitored by a K type thermocouple spot-welded to the back of the sample (Ta) or to the sample holder pressed to the sample backside (Al and Cu). The manipulator allowed

liquid nitrogen cooling to 80 K and resistive heating to 1500 K for Ta and 800 K for Al and Cu.

Sample cleaning was performed by Ar^+ ion bombardment at 2 keV beam voltage. The surface was cleaned by cycles of Ar ion sputtering and annealing to 700 K for Al and Cu, and 1100 K for Ta. Impurities on Al and Cu were readily removed by this procedure and sample cleanness was verified by AES. However, the procedure was only sufficient to remove most of the surface impurities from Ta. The high solubility of oxygen in Ta caused a diffusion of oxygen from the bulk to the surface upon annealing to elevated temperatures. Complete removal of carbidic/graphitic carbon was also not accomplished because it would require heating to above 2000 K (24), which was not possible in the manipulator setting. The typical well-sputtered and annealed Ta surfaces used for the experiments have submonolayer coverages of oxygen and carbon.

Vinyl-silane precursors were introduced directionally through manual leak valves and stainless steel doser tubes. Dosing was carried out using commercially available VTMS (97%, Aldrich) and VTCS (97%, Aldrich). Both precursors are liquids at room temperature and were purified by several freeze- pump-thaw cycles prior to distillation into the vacuum chamber. Exposures were determined by monitoring background pressure and time of exposure (1 Langmuir (L) = 10^{-6} Torr-sec) and have not been corrected for the effects of ion gauge sensitivity, flux to the sample or directional dosing.

Electron bombardment of adsorbed species was accomplished using the co-axial Auger electron gun with 500 eV electron energy. The electron beam was defocused to the maximum extent (estimated spot size 0.2 cm^2) and the filament emission current kept

at 1mA. The current the sample received during the bombardment was approximately 1 μA as measured by a picoammeter. The corresponding electron flux to the sample surface calculated under these conditions is $3\times10^{13}/cm^2s$. Due to the secondary electron emission from the sample, the actual flux should be greater than this value.

Ultraviolet (UV) photon radiation was performed by a 500 watt Hg(Xe) arc lamp (Oriel, Model 66142) placed outside the UHV chamber. It has a continuous output from 200-800 nm wavelength, with intense Hg peaks in the UV-visible and Xe lines in the near-infrared region. The collimated beam was admitted onto the sample though a UV-transparent quartz viewport. The beam spot was adjusted to cover the entire sample and the distance between the source and the sample was about 5 cm.

Cu evaporation was performed with a home-built evaporator that consisted of a W filament wrapped with a Cu strip. Evaporation was conducted by controlling the heating current and the evaporation time.

2.3. Results and Discussions

2.3.1. Interaction of precursors with Metal Substrates

AES and TPD studies were carried out to characterize the thermal stability and reactivity of vinyltrichlorosilane (VTCS) on Al and Cu surfaces.

The relative surface concentrations for Si, C and Cl on Al (calculated by Equation (2-1)) at different VTCS coverages at room temperature are listed in Table 2.1. It can be seen that for a wide range of VTCS coverage (5-100 L), the surface concentrations of Si, C and Cl remain relatively the same. This indicates that the adsorption of VTCS on Al at room temperature saturates at 5 L. The average Si:C:Cl

ratio (1:1.8:2.5) is close to the stoichiometry of VTCS precursor (1:2:3), however, it is hardly meaningful since the individual ratio at each coverage varies greatly. The standard deviation values (~30%) are well above the possible error range (~15%) of Auger measurement. A possible explanation is that the adsorption is dissociative, with similar fragmentation pathways at different coverages, leading to different surface compositions.

Table 2.1. Relative surface concentrations for Si, Cl and C on Al at different CTCS coverages at room temperature

VTCS Coverage (L)	Si	C	Cl	Si:C:Cl
5	0.082	0.10	0.14	1:1.2:1.7
10	0.075	0.14	0.19	1:1.9:2.5
20	0.075	0.10	0.16	1:1.3:2.1
70	0.075	0.19	0.32	1:2.5:4.3
100	0.10	0.19	0.21	1:1.9:2.1
Average	0.081±0.01	0.14±0.04	0.20±0.06	1:(1.8±0.5):(2.5±0.9)

Only H_2 (amu 2) desorption was detected from TPD (anneal to 700 K) studies for all coverages as is shown in Figure 2.3(a). All the desorptions occurred at the temperature range of 470-650 K with the peaks at about 540 K. The area under the desorption peaks are plotted in Figure 2.3(b). It can be seen that the area stays roughly the same for different VTCS coverage, with the exceptionally small desorption at 10 L.

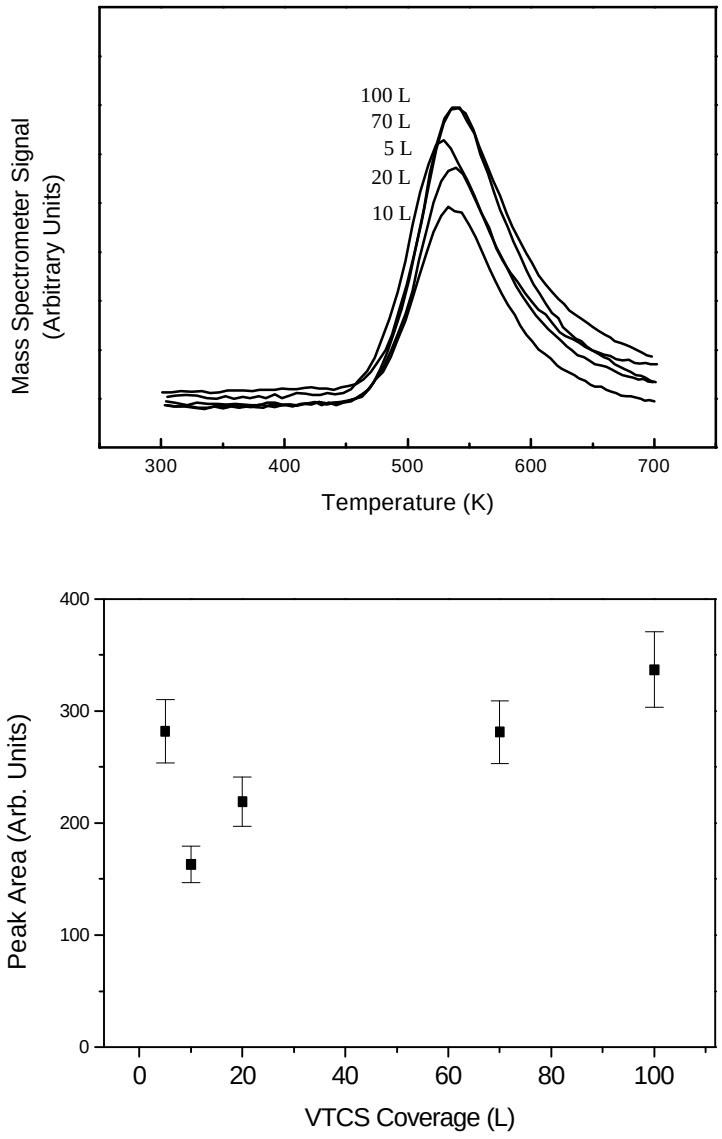

Figure 2.3. (a) H_2 (amu 2) desorptions from a Al surface with different initial VTCS coverages at room temperature, (b) the area under the H_2 desorption peaks with different VTCS coverages.

This again indicates that the adsorption of VTCS on Al saturates at 5 L. Auger spectra taken after TPD reveal the complete disappearance of Si and less than 0.02

concentrations of C and Cl on the surface for all coverages. This shows a weak interaction and poor thermal stability of VTCS on Al.

The adsorption of VTCS on Cu at room temperature was studied in a similar manner. Due to the interference of Cu transitions at 60 and 105 eV, it is hard to quantify the surface concentration of Si (92eV) in this system by AES. The surface composition after VTCS adsorption, therefore, was not calculated. VTCS adsorption behavior on Cu at room temperature, expressed in Cl/Cu atomic ratios, is shown in Figure 2.4.

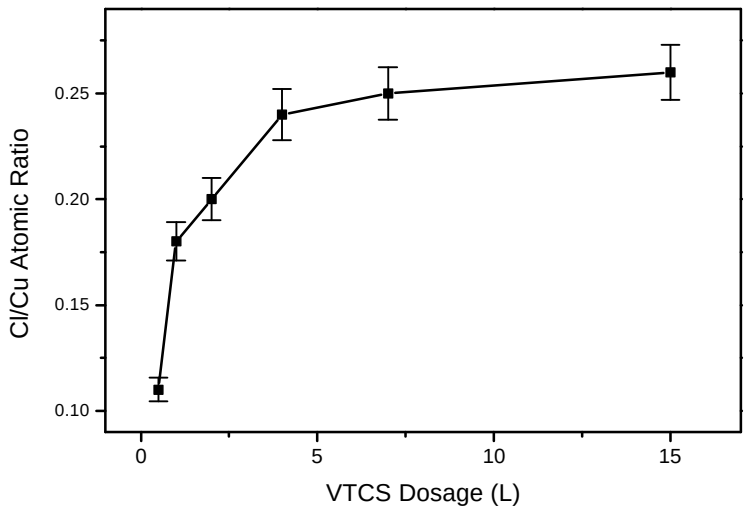

Figure 2.4. Cl/Cu atomic ratio as a function of VTCS exposure on Cu at room temperature.

It can be seen that the concentration of Cl on Cu increases rapidly with initial VTCS exposures until it saturates at about 5 L. This saturation coverage can be considered as a monolayer of adsorped VTCS, where it reaches a Cl/Cu ratio of ~ 0.25. This value is almost twice that of Cl/Al at the same VTCS coverage. These results indicate that the

sticking coefficient of VTCS on Cu is greater than Al at room temperature. No significant desorptions were detected from TPD studies. Auger spectra taken after TPD (700 K) show roughly the same amount of Cl and C surface concentrations, indicating also stronger interaction of VTCS with Cu than Al.

2.3.2. Formation of Films

Even though there is some difference between the interaction of VTCS with Al and Cu at room temperature, the sticking coefficient in both cases is too small for film growth. In order to form a thick layer of VTCS precursors on the metal substrates, the adsorption needs to be carried out at low temperature. After the samples were cooled down to 80-90 K, 0.05 L VTCS was introduced on to the surfaces. Because of the enhancement factor of directional dosing and the high sticking coefficient (considered unity) at such low temperature, even 0.05 L of the precursors formed an ad-layer that was thick enough to attenuate the substrate signals. According to Equation (2-2), attenuation of the substrate signal to 1% of its original would require an over-layer equal to a thickness about five times the mean free path of the substrate Auger electron (5-10 Å) (25). Therefore 100 Å is a conservative estimate of the thickness of the over-layer. The different desorption behaviors of VTCS with or without electron/photon bombardment were studied by AES and TPD.

TPD results are shown in Figure 2.5 for 0.05 L VTCS adsorbed on clean Al at 90 K, and then desorbed from the surface without (a) or with (b) electron bombardment prior to the thermal ramp. It can be observed from Figure 2.5(a) that VTCS desorbs molecularly from the surface near 200 K in the absence of electron bombardment. No

desorption was detected above 250 K. In contrast, exposure to electron flux, as shown in Figure 2.5(b), results in much less desorption of the same species over an extended temperature range. Significantly, no desorption of the vinyl group-containing fragment, CH_2=$CHSiCl_2^+$ (amu 125) is observed, although this species is prominent in the desorption spectrum in the absence of electron bombardment. These results indicate that electron bombardment has induced reaction of the vinyl group.

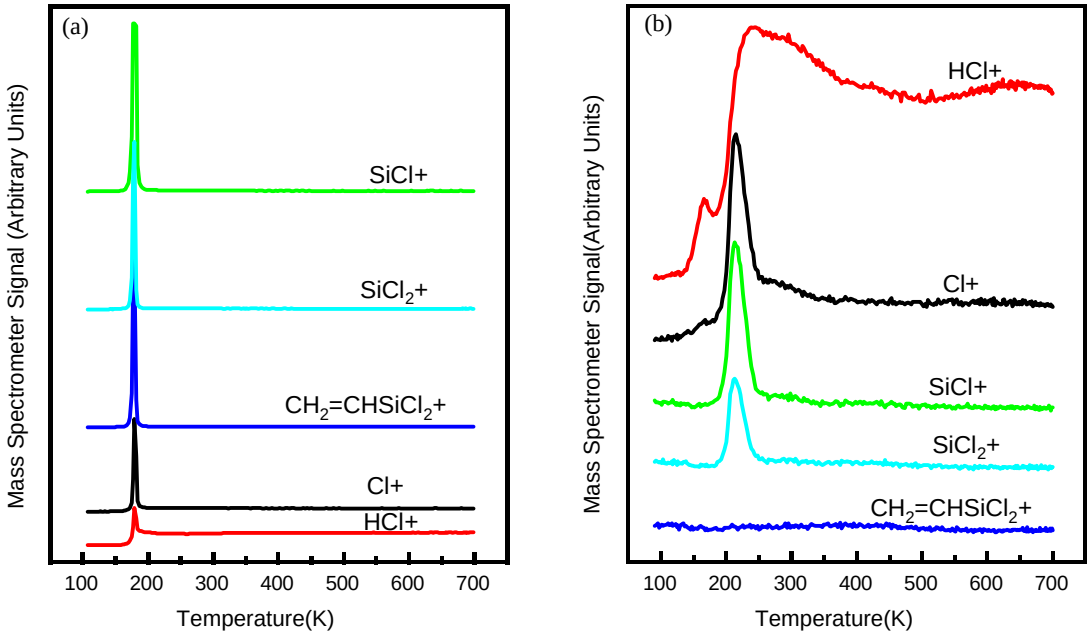

Figure 2.5. TPD spectra of 0.05 L VTCS adsorped on Al at 90 K (a) without and (b) with electron bombardment (3 × 10 13 /cm2 s for 10 min) prior to sample heating.

The corresponding Auger spectra are shown in Figure 2.6. Deposition of 0.05 L VTCS completely obscures the Al substrate signal, suggesting a multilayer coverage of the precursors, as shown in Figure 2.6(a). Auger spectrum taken after annealing to 700 K

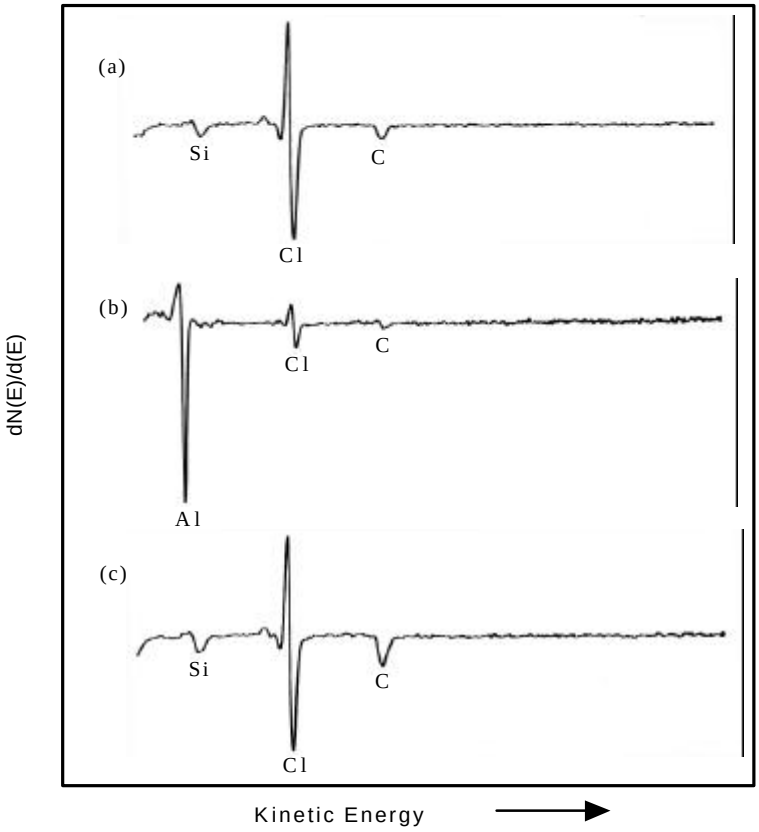

Figure 2.6. Auger spectra of (a) VTCS multilayer adsorbed at 90 K on Al; (b) VTCS multilayer adsorbed at 90 K and annealed to 700 K without electron bombardment; and (c) VTCS multilayer adsorbed at 90 K, subjected to electron bombardment (3×10^{13}/cm^{2}s for 10 min), and annealed to 700 K.

reveals minor amounts of Si, C, and Cl left on the surface and a distinct increase of the Al substrate signal, as shown in Figure 2.6(b). The relative atomic concentrations of Si, C and Cl are less than 5% compared to Al. These results indicate low reactivity of Al with VTCS below the desorption temperature of 200 K. The effect of electron bombardment is demonstrated in Figure 2.6(c). It can be seen that electron bombardment prior to annealing results in the formation of a polymeric film that is adherent and stable on the

substrate to the temperature of 700 K. The film had a Si:Cl:C ratio of 1:3:2 as determined by relative concentrations of surface species. This composition is the same as that observed for the molecularly adsorbed multilayer at 90 K, and the same as that of the molecular precursor.

Similar experiments were performed on a Cu substrate. TPD results of 0.05 L VTCS adsorped on Cu at 80 K are shown in Figure 2.7. The effect of electron beam is clearly demonstrated by the difference in the two spectra.

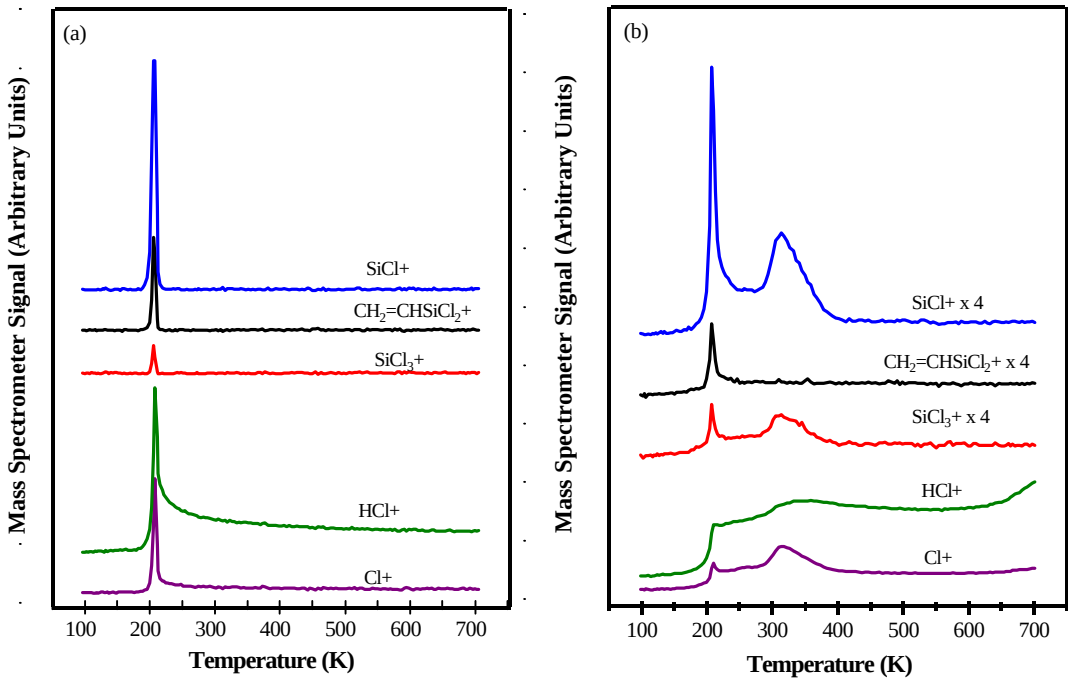

Figure 2.7. TPD spectra of 0.05 L VTCS adsorped on Cu at 80 K (a) without and (b) with electron bombardment (3×10^{13} /cm^2 s for 10 min) prior to sample heating.

VTCS desorps molecularly at 200 K without the electron pre-treatment, as shown in Figure 2.7(a). The molecular desorptions can still be seen in Figure 2.7(b) after the electron beam bombardment, but to much less extent, indicating the presence of small amount of non-polymerized VTCS precursors. A second desorption feature appeares at above 300 K for all the cracking patterns of VTCS except for the vinyl containing moiety CH_2=$CHSiCl_2^+$ (amu 125). This implies that the crosslinking is accomplished through the vinyl group and the process is complete below room temperature.

Corresponding Auger spectra are shown in Figure 2.8. It can be seen from Figure 2.8(a) that depositing 0.05 L VTCS at 80 K produces an over-layer thick enough to completely attenuate the Cu Auger signal. Heating the sample subsequently to 700 K causes most of the precursors to desorb, as shown in Figure 2.8(b). Surface concentration calculations reveal that the Cl/Cu atomic ratio after heating up to 700 K is 0.25, which is exactly the same as that of the saturation dosage at room temperature (Figure 2.4). This means that condensing VTCS at 80 K forms a multilayer on Al which is subsequently desorbed upon heating, leaving the same monolayer coverage of VTCS as obtained from dosing it at room temperature. Electron beam treatment has proved to improve the adhesion of VTCS on Cu as shown in Figure 2.8(c). After annealing to 700 K, the substrate is still completely covered by VTCS film and the chemical composition of the film remains the same ratio (Si:Cl:C ≈ 1:3:2).

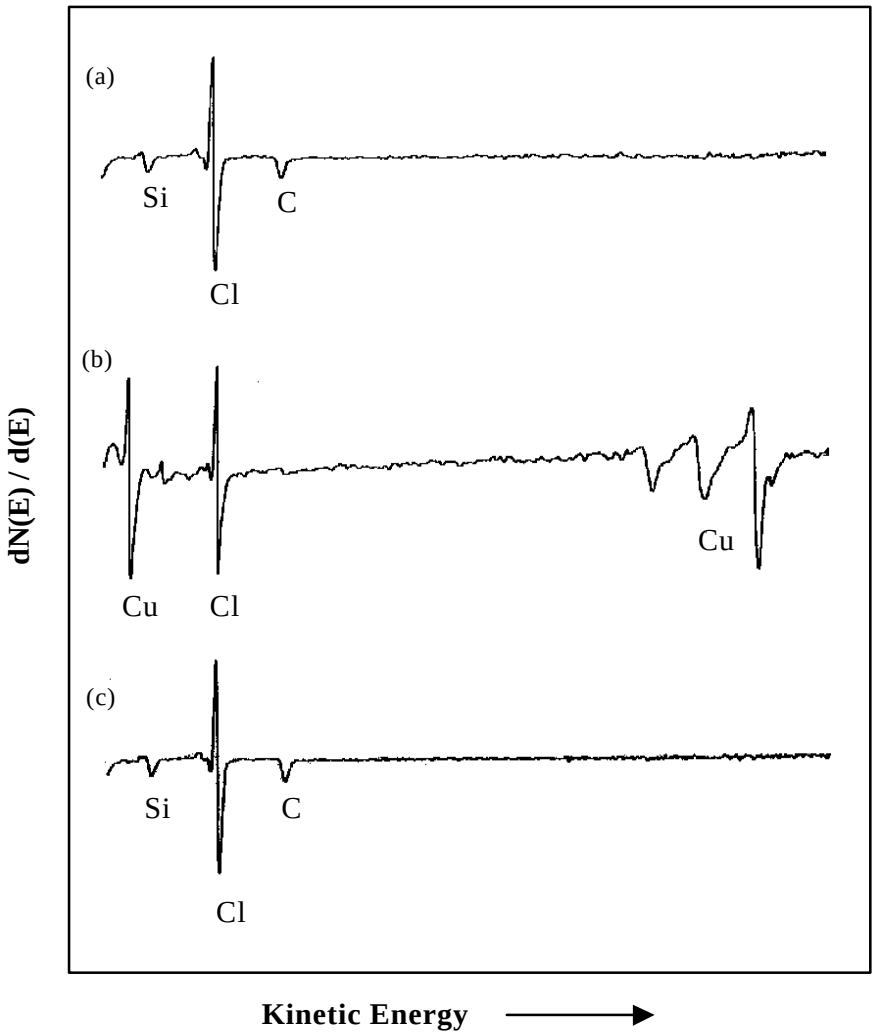

Figure 2.8. Auger spectra of (a) VTCS multilayer adsorbed at 80 K on Cu; (b) VTCS multilayer adsorbed at 80 K and annealed to 700 K without electron bombardment; and (c) VTCS multilayer adsorbed at 80 K, subjected to electron bombardment (3×10^{13}/cm^{2}s for 10 min), and annealed to 700 K.

The effect of UV photon radiation on the adsorped VTCS precursors was studied by condensing 0.3 L of VTCS on Al at 90 K followed by 30 min of UV bombardment. A slight temperature increase (less than10 K) was observed during the treatment.

Essentially identical TPD results were obtained as compared to electron beam bombardment. Auger spectra taken before (Figure 2.9(a)) and after (Figure 2.9 (b)) TPD (700 K) indicate that the composition of the VTCS over-layer does not change after UV radiation. However, thermal annealing causes the reduction of film thickness as evidenced by the appearance of Al substrate signal in Figure 2.9(b). These results suggest that UV radiation can also induce polymerization of the precursors but under the current experimental conditions, it was not as effective as the electron bombardment.

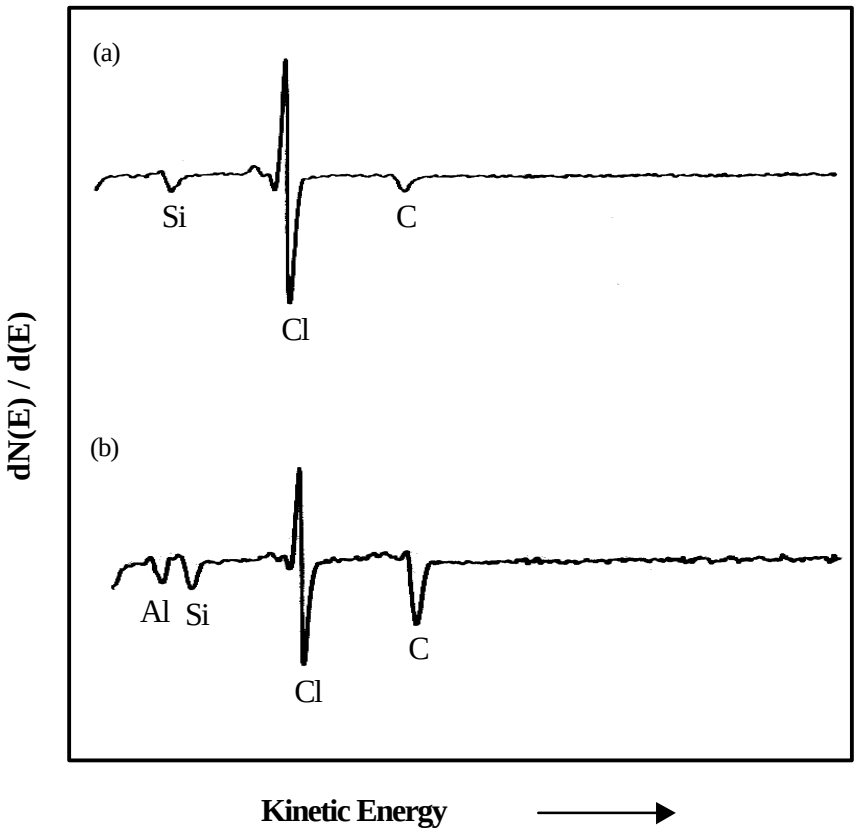

Figure 2.9. Auger spectra of 0.3 L VTCS adsorpted on Al at 90 K followed by 30 min UV radiation (a) before and (b) after annealing to 700 K.

2.3.3. Thermal Stability of the Film

Results from the previous section have shown that VTCS-derived films are thermally stable at 700 K on Al and Cu. In order to test the thermal stability of the films at higher temperatures, Ta was chosen as the substrate. Since Ta has a higher electrical resistivity (13.5×10^{-8} Ωm at 300 K) than Al (2.733×10^{-8} Ωm at 300 K) and Cu (1.725×10^{-8} Ωm at 300 K) (26), it allows better resistive heating with the same amount of current passing through the sample. A thin C-Si film was formed on Ta by successive condensation and electron beam bombardment of another vinyl silane precursor, vinyltrimetheylsilane (VTMS). Successive depositions permitted the gradual build-up of a film until the Ta Auger signal can no longer be observed, suggesting an average film thickness of about 100 Å (25). The thermal stability of the electron beam-induced VTMS film on Ta is demonstrated in Figure 2.10, which shows the film as formed at 80 K, and successively annealed to higher temperatures.

The film has a Si:C ratio of 1:4 as determined by Auger intensity and relative sensitivity factors. This composition is, again, similar to that of the precursor (1:5). The Ta substrate Auger signal remains completely attenuated until the film was annealed to 1000 K, indicating the thickness of the film remained about 100 Å until 1000 K, when signal from the Ta substrate is observed. The Si:C ratio also remains stable until annealed to 1100 K when the structure of the film is completely altered with the Si:C ratio reduced to 1:1. At this point, the C signal assumes the three-lobed line shape characteristic for carbidic carbon species (23), indicating the formation of silicon carbide or tantalum carbide.

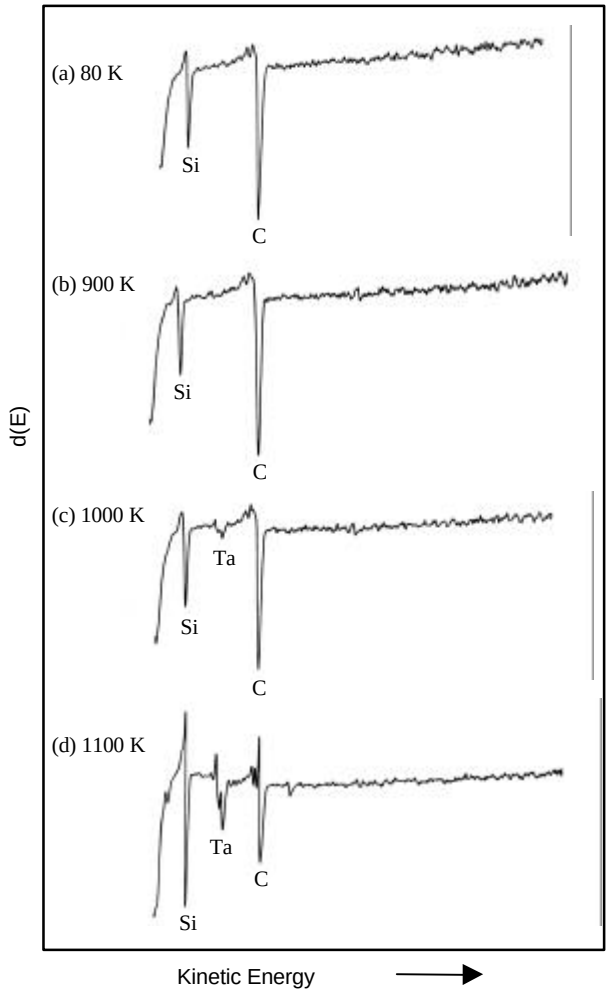

Figure 2.10. Auger spectra of 0.05L VTMS adsorbed on Ta, subjected to electron bombardment (3×10^{13}/cm^{2}s for 10 min) at (a) 80 K, and annealed to (b) 900 K, (c) 1000 K, and (d) 1100 K.

2.3.4. Stability to H_2O

The reactivity of these films to H_2O molecules was tested by condensing a small exposure (0.01 L) of H_2O onto the films at 80 K followed by TPD to higher temperatures (700-800 K for Al and Cu substrates, and 1000 K for Ta substrates). Auger

measurements were taken after each TPD to examine the stability of the films with respect to H_2O vapor.

The Auger spectrum of a VTCS derived-film on Cu substrate after 10 cycles of TPD is shown is Figure 2.11. Decrease of the Si, Cl and C Auger signals is observed together with increase of O and the Cu substrate signal. It can also be noticed that the Si:Cl:C ratio is no longer 1:3:2, indicating the destruction of the film structure. A closer look at the Auger result revealed that the decrease in Cl signal intensity is much more pronounced than those of Si and C.

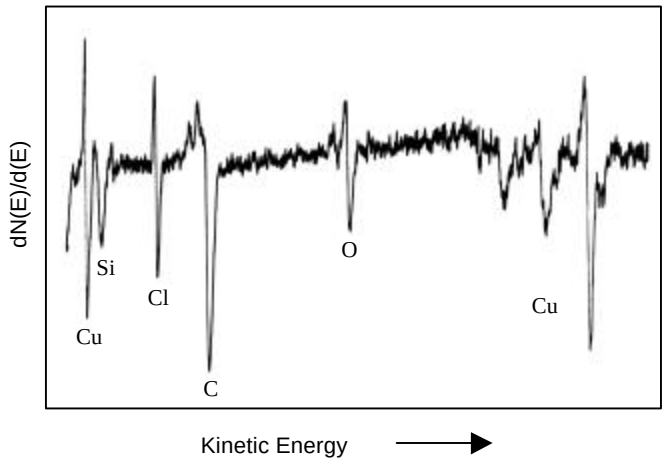

Figure 2.11. Auger spectrum of a VTCS derived film on Cu after 10 cycles of TPD with 0.01 L H_2O.

Corresponding TPD results are shown in Figure 2.12. Essentially identical results were obtained for all 10 cycles of experiments. Appreciable amounts of HCl and Cl desorptions are observed apart from the expected H_2O desorption. This explains the

rapid decrease of Cl intensity from the Auger results. It also implies that the Cl group is the main reason for the VTCS-film's susceptibility to moisture.

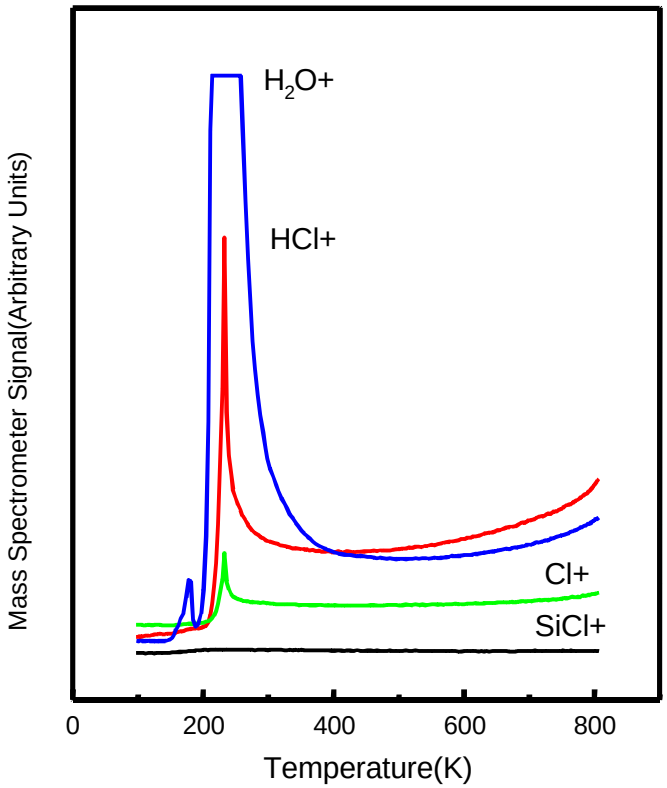

Figure 2.12. TPD spectra of 0.01 L H_2O adsorpted at 80 K on a VTCS-derived film on Cu.

Similar experiments were conducted on a VTMS-derived film on Ta. Since this precursor does not contain Cl, it is expected to display better resistivity to water. In fact only H_2O and H_2 desorptions were detected in the TPD spectra, whereas no desportion of any of the VTMS fragments were observed. After carrying out the procedure 10 times, still no Ta substrate signal from the Auger was observed, as demonstrated in Figure 2.13.

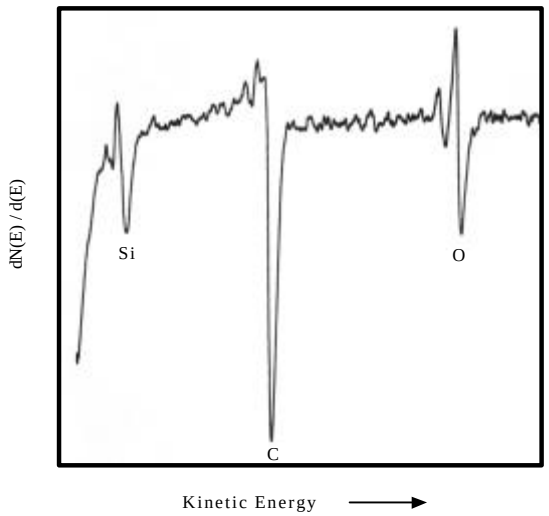

Figure 2.13. Auger spectrum of a VTMS-derived film on Ta after 10 cycles of TPD with 0.01 L H_2O.

The Auger results also show an initial steep increase of O content in the film, which begins to level after several reaction cycles with H_2O. The O content in the film represented by the atomic ratios of O/Si and O/C is plotted in Figure 2.14 against the number of TPD with H_2O. Both ratios reach a plateau after the seventh reaction with a value of O/Si ≈ 1 and O/C ≈ 0.2. Considering the chemical composition of the film (Si:C ≈ 1:4), this leaves roughly one H_2O molecule per VTMS unit when the uptake of water saturates. The exact mechanism for this process is unclear but it implies that H_2O molecules can only occupy certain sites on the VTMS-derived film.

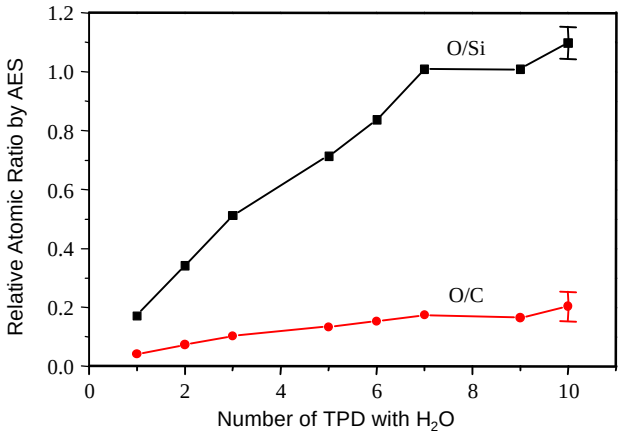

Figure 2.14. O/Si and O/C atomic ratio by AES as a function of increasing number of TPD with 0.01 L H_2O on VTMS-derived film on Ta.

2.3.5. Cu Thermal Diffusion

The effectiveness of these films against Cu thermal diffusion was first tested by annealing a VTCS-derived film on Cu to elevated temperatures. Annealing to 850 K yields the following Auger spectrum shown in Figure 2.15.

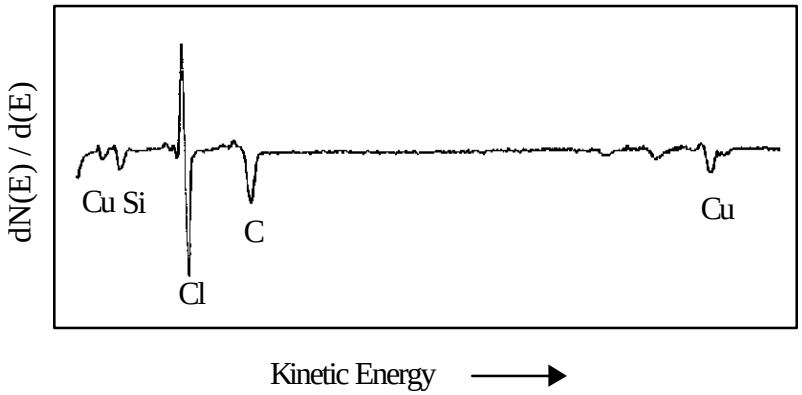

Figure 2.15. Auger spectrum of a VTCS-derived film on Cu annealed to 850 K.

It can be seen that the chemical composition of the film does not change much according the Si:Cl:C ratio, but Cu substrate signal appears, indicating that either the thickness of the film decreases or Cu diffuses through the film at 850 K.

In order to clarify the thermal interaction of Cu with these films, Cu over-layers were formed on these films and annealed to elevated temperatures. The barrier property of VTMS-derived films against Cu thermal diffusion was tested on both Al and Ta substrates. After the formation of a roughly 100 Å thick VTMS-derived polymer film at 80-90 K, Cu was deposited on the film by thermal evaporation at the same low sample temperature. The Auger peak-to-peak intensity ratios of Cu(920eV)/Si(92eV) and Cu(920eV)/Cu(60eV) were monitored as the sample was annealed to progressively higher temperatures in UHV.

The result of VTMS on an Al substrate is shown in Figure 2.16. The relative Cu/Si intensity remains unchanged until 300 K. It decreases by about 25% between 300 K and 600 K. Above 600 K, it decreases precipitously. In order to determine whether the decrease in Cu intensity above 400 K is in fact due to Cu diffusion, the AES intensity ratio of Cu(920eV)/Cu(60eV) as a function of temperature is also shown in Figure 2.16. Because of the different mean free paths of Auger electrons resulting from these two Auger transitions -- approximately 18 Å for the Cu(920eV) transition and 4 Å for the Cu(60eV) transition (25) -- the Cu signal at 60 eV is more surface sensitive. Therefore, diffusion of the Cu over-layer into the bulk should produce an increase in the ratio of Cu(920eV)/Cu(60eV) and this has been observed for Cu diffusion into alumina (27). As demonstrated in Figure 2.16, there is no significant change of this ratio throughout the

whole temperature range. The decrease in relative Cu/Si intensity above 300 K, therefore, is attributed to de-wetting: the formation of 3-dimensional nuclei on the Cu surface in a transition from conformal coverage.

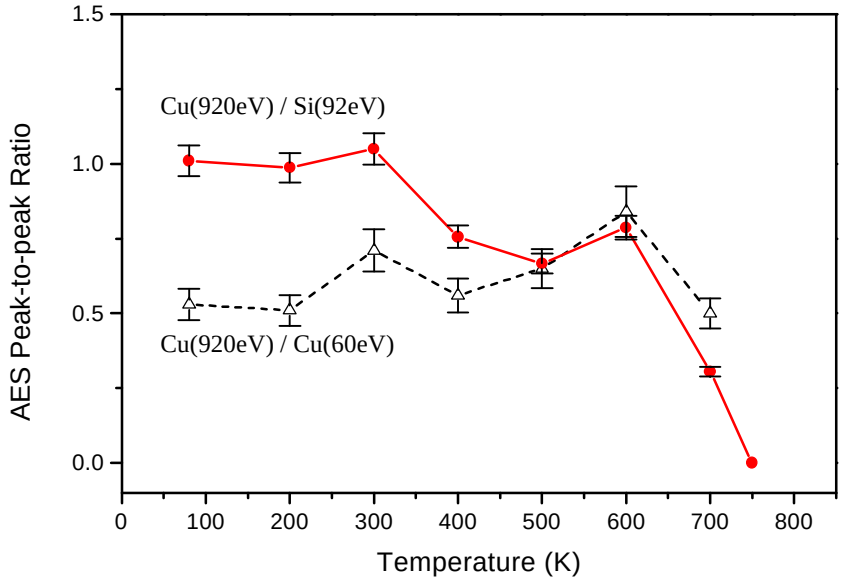

Figure 2.16. Relative Auger intensity ratios as a function of sample temperature for a VTMS-derived film on Al substrate, followed by evaporative deposition of Cu at 90 K.

In order to completely rule out the possibility that the decrease in Cu intensity was due to diffusion, Cu was deposited at 90 K on a new VTMS-derived film on Al. The sample was annealed to 600 K for prolonged time periods. The results of this experiment are shown in Figure 2.17. During the first 5 min annealing, there is an initial 50% decrease in the Cu/Si ratio. No further decrease is observed up to the 60 min annealing period at 600 K. Furthermore, the Cu(920eV)/Cu(60eV) ratio remains constant

throughout the annealing time. These results indicate that annealing to 600 K causes a change in the conformation of the Cu over-layer, but not diffusion into the bulk.

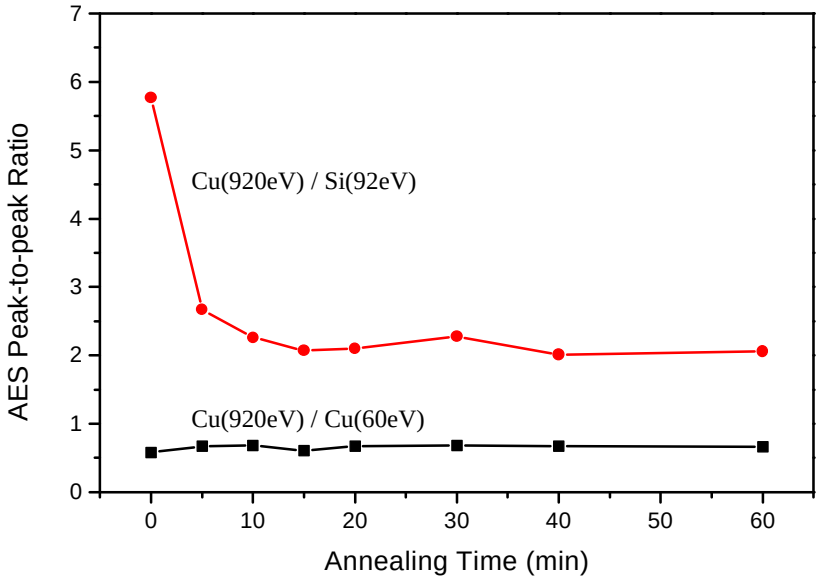

Figure 2.17. Relative Auger intensity ratios as a function of annealing time at 600 K for a VTMS-derived film on Al substrate, followed by evaporative deposition of Cu at 90 K.

Similar experiments were conducted on a Ta substrate, which enables the thermal annealing to higher temperatures. The results are shown in Figure 2.18. It can be seen that the Cu/Si ratio starts to decrease steadily from 400 K. The Cu(920eV)/Cu(60eV) ratio, on the other hand, remains stable until the sample is heated above 800 K, indicating that TMVS-derived film has effectively blocked the thermal diffusion of Cu up to 800 K. The decrease in relative Cu/Si intensity from 300 to 800 K is, again, caused by Cu de-wetting from the surface.

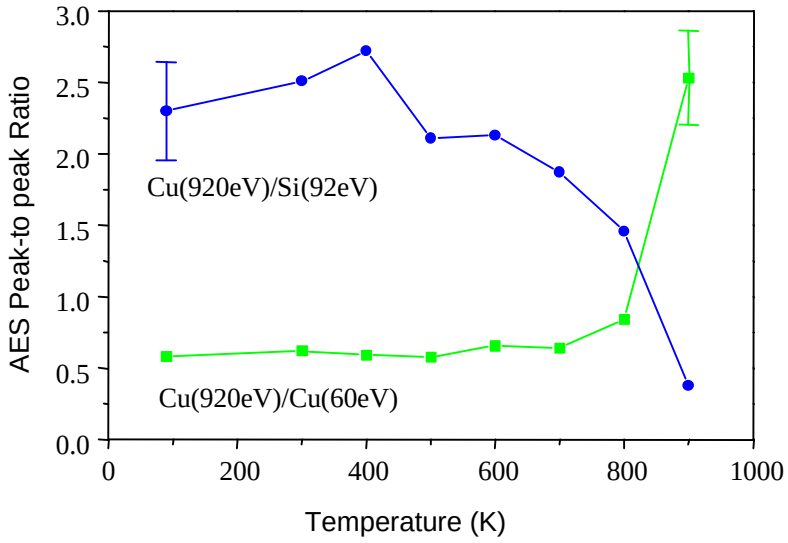

Figure 2.18. Relative Auger intensity as a function of sample temperature for 0.05L VTMS adsorbed on Ta, subjected to electron bombardment (3×10^{13}/cm^{2}s for 10 min) at 80 K, followed by evaporative deposition of Cu at 80 K: Cu starts to diffuse above 800 K.

2.3.6. Incorporation of Hexafluorobenzene

In order to determine if fluoropolymers or precursors could be incorporated into these films, different amounts of hexafluorobenzene (C_6F_6) were condensed on a 0.1 L VTCS multilayer on a clean Cu substrate at 80 K. The condensed multilayers were then subjected to electron beam bombardment (3×10^{13}/cm^{2}s for 10 min) at 90 K and TPD was carried out to 700 K.

TPD results for the incorporation of 0.07 L C_6F_6 into VTCS film are shown in Figure 2.19. Again, very little desorption of the vinyl-containing species CH_2=$CHSiCl_2^+$ (amu 125) is observed, indicating the crosslinking through the vinyl groups during the electron beam bombardment. Other fragments from the VTCS and C_6F_6 molecules also

desorb at ~220 K. A second desorption of one of the VTCS fragments, $SiCl^+$ (amu 63) is also detected as a broad peak in the 280-400 K region. The dependence of this peak on the amount of C_6F_6 condensed on 0.1 L VTCS is plotted in Figure 2.20. At lower dosages of C_6F_6, this peak appears as a shoulder to the 220 K desorption. It grows with increasing C_6F_6 dosages and becomes separated from the 220 K peak. These results indicate the interaction between the two ad-layers, which in turn, should promote the adhesion of the C_6F_6 layer.

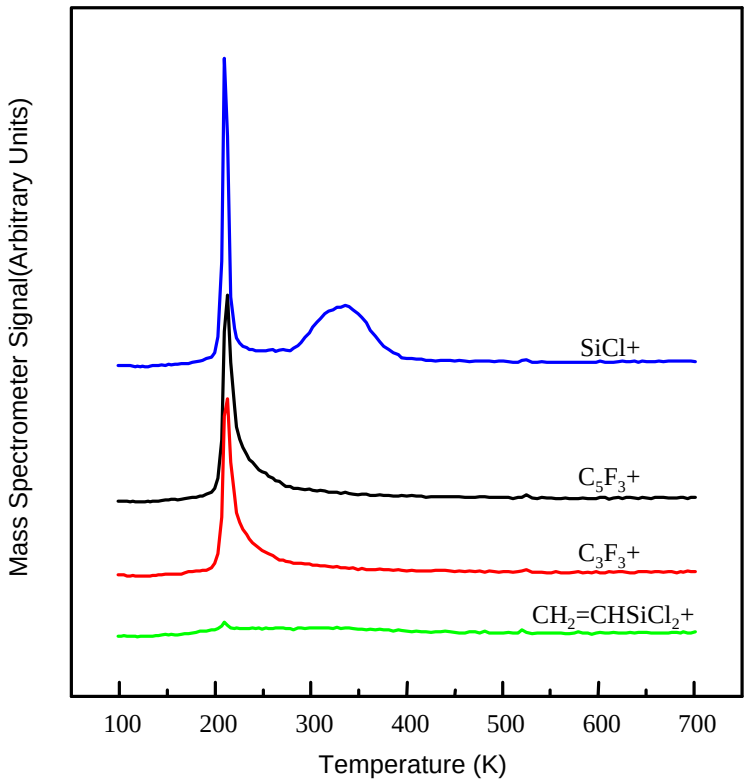

Figure 2.19. TPD spectra for 0.07 L C_6F_6 and 0.1 L VTCS co-adsorbed on Cu, subjected to electron bombardment ($3\times10^{13}/cm^2s$ for 10 min) at 80 K prior to sample heating.

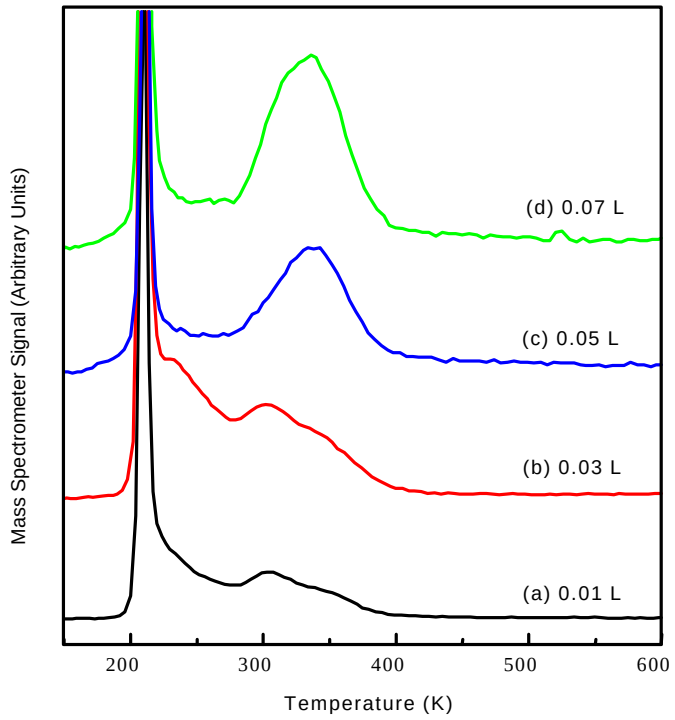

Figure 2.20. TPD spectra of $SiCl^+$ (amu 63) for different amount of C_6F_6 co-adsorbed with 0.1 L VTCS on Cu, subjected to electron bombardment (3×10^{13}/cm^{2}s for 10 min) at 80 K prior to sample heating.

Auger spectrum recorded after the TPD (Figure 2.21) indicates a stable and adherent film that completely attenuates the Cu substrate. Furthermore, it also shows the presence of F, plus a C Auger lineshape (the insert of Figure 2.21) characteristic of graphite or an aromatic ring system (28). This line shape is distinctly different from that observed in the absence of C_6F_6 and indicates the incorporation of an aromatic ring in the structure. The details of the perfluorobenzene film environment, however, cannot be discerned from Auger analysis.

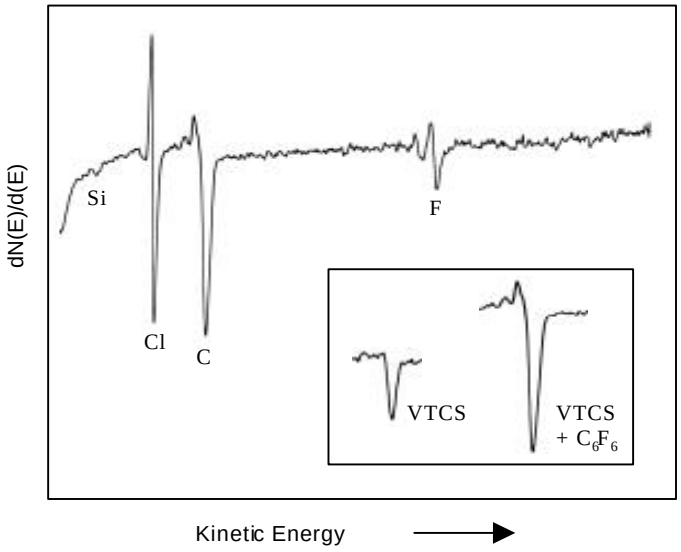

Figure 2.21. Auger spectrum of a film prepared via co-adsorption of 0.1 L C_6F_6 and 0.01 L VTCS on Cu with electron bombardment ($3\times10^{13}/cm^2s$ for 10 min) at 80 K. The insert shows the different C Auger line shape from a VTCS-derived film and a VTCS+ C_6F_6 – derived film.

2.4. Summary and Conclusions

The results shown here indicate that electron beam or UV radiation can induce cross-linking in condensed multilayers of vinylsilane derivative monomers, resulting in polymeric C-Si films that are thermally stable on Al, Cu, and Ta substrates to elevated temperatures. Preliminary data also indicate that such films are promising Cu diffusion barriers and adhesion promoters for, e.g., plasma deposited fluoropolymer films or related materials. The thermal diffusion temperature of Cu on these films (> 800 K) is comparable to those of Ta substrates (29) and the de-wetting temperature (400 K) is the same as oxygen modified Ta (30). It is also possible to incorporate fluoropolymers into the film by introducing fluorine-containing precursors during the growth. In this respect

it should be pointed out that the adhesion/diffusion barrier characteristics of this class of materials may well be selectively variable through the appropriate choice of monomer precursors.

There are a number of issues to be addressed, including the deposition of C-Si films at 300 K or above, as commonly encountered in industrial practice. The potential to deposit adherent films on Cu substrate is high, as silane reaction with Cu surfaces to form Cu-Si bonds is known to be an activated process which occurs readily at or above 300 K (31), even in the absence of radiation. Studies to further quantify the diffusion barrier characteristics of such films at ultra-thin thicknesses are underway in our laboratories. Recent XPS results (32) indicate that VTMS-derived films are stable in air, which enables the films to be taken out of UHV for electronic tests such as capacitance measurements.

2.5. Chapter References

(1) *The National Technology Roadmap for Semiconductors: Technology Needs*; Semiconductor Industry Association: San Jose, CA, 1997.

(2) Ono, H.; Nakano, T.; Ohta, T. *Appl. Phys. Lett.* **1994,** *64,* 1511.

(3) Hu, C.-K.; Chang, S.; Small, M. B.; Lewis, J. E. *Proceedings of the International VLSI Multilevel Interconnection Conference* **1986**, 181-187.

(4) Reid, J. S.; Kolawa, E.; Ruiz, R. P.; Nicolet, M.-A. *Thin Solid Films* **1993,** *236,* 319-324.

(5) Stavrev, M.; Fischer, D.; Preub, A.; Wenzel, C.; Mattern, N. *Microelectronic Eng.* **1997,** *33,* 269-275.

(6) Wang, M. T.; Lin, Y. C.; Chen, M. C. *J. Electrochem. Soc.* **1998,** *145*, 2538.

(7) Wong, S. S.; Ryu, C.; Lee, H.; Kwon, K.-W. *Mater. Res. Soc. Symp. Proc.* **1998,** *514*, 75.

(8) Ryan, E. T.; McKerrow, A. J.; Leu, J.; Ho, P. S. *MRS Bull.* **1997,** *22*, 49.

(9) Sacher, E. *Prog. Surf. Sci.* **1994,** *4*, 273.

(10) Raghavan, G.; Chiang, C.; Anders, P. B.; Tzeng, S.-M.; Villasol, R.; Bai, G.; Bohr, M.; Fraser, D. B. *Thin Solid Films* **1995,** *262*, 168.

(11) Park, J. M.; Matienzo, L. J.; Spencer, D. F. *J. Adhersion Sci. Technol.* **1991,** *5*, 153.

(12) Loke, A. L. S.; Ryu, C.; Yue, C. P.; Cho, J. S. H.; Wong, S. S. *IEEE Electron Device Lett.* **1996,** *17*, 549.

(13) Tillman, N.; Ulman, A.; Penner, T. L. *Langmuir* **1989,** *5*, 101-111.

(14) Wasserman, S. R.; Tao, Y.-T.; Whitesides, G. M. *Langmuir* **1989,** *5*, 1074-1087.

(15) Kurth, D. G.; Bein, T. *Langmuir* **1995,** *11*, 578-584.

(16) Kurth, D. G.; Bein, T. *J. Phys. Chem.* **1992,** *96*, 6707-6712.

(17) Gamble, L.; Jung, L. S.; Campbell, C. T. *Langmuir* **1995,** *11*, 4505-4514.

(18) Xu, J.; Choyke, W. J.; Yates, J. T. J. *Appl. Surf. Sci.* **1997,** *In Press.*

(19) Mountsier, T. W.; Kumar, D. *Mat. Res. Soc. Symp. Proc.* **1997,** *443*, 41.

(20) Du, M.; Opila, R. L.; Donnelly, V. M.; Sapjeta, J.; Boone, T. *J Appl. Phys.* **1999,** *85*, 1496.

(21) Chen, L.; Kelber, J. A. *Low-Dielectric Constant Materials IV*, San Francisco 1998; Materials Research Society; 297.

(22) Chen, L.; Kelber, J. A. *J. Vac. Sci. Technol. A.* **1999,** *17*, 1968.

(23) Davis, L. E.; MacDonald, N. C.; Palmberg, P. W.; Riach, G. E.; Weber, R. E. *Handbook of Auger Electron Spectroscopy*, Second ed.; Physical Electronics Industry, Inc.: Eden Prairie, Minnesota, 1976.

(24) Musket, R. G.; McLean, W.; Colmenares, C. A.; Makowiecki, D. M.; Siekhaus, W. J. *Appl. Surf. Sci.* **1982,** *10*, 143-207.

(25) Somorjai, G. A. *Introduction to Surface Chemistry and Catalysis*; John Wiley & Sons, Inc., 1994.

(26) Lide, D. R. *CRC Handbook of Chemistry and Physics*, 74th ed.; CRC Press, Inc., 1993.

(27) Chen, J. G.; Colaianni, M. L.; Weinberg, W. H.; J T Yates, J. *Surf. Sci.* **1992,** *279*, 223-232.

(28) Bhattacharya, A. K. *J. Mol. Catal.* **1994,** *99*, 181.

(29) Clevenger, L. A.; Bojarczuk, N. A.; Holloway, K.; Harper, J. M. E.; C Cabral, J.; Schad, R. G.; Cardone, F.; Stolt, L. *J. Appl. Phys.* **1993,** *73*, 300.

(30) Chen, L.; Ekstrom, B.; Kelber, J. *Mater. Res. Soc. Symp. Proc.* **1999,** *564*, in press.

(31) Wiegand, B. C.; Lohokare, S. P.; Nuzzo, R. G. *J. Phys. Chem.* **1993,** *97*, 11553-11562.

(32) Martini, D.; Kelber, J. A. **unpublished results**.

CHAPTER 3

EFFECT OF SURFACE IMPURITIES ON THE COPPER/TANTALUM INTERFACE

3.1. Introduction

Refractory metals have been recognized as potential diffusion barriers for Cu interconnects because of their high thermal stability and good electrical conductivity (1-6). Investigations are generally carried out by studying the thermal stability of a Cu/M/Si (M = refractory metals) sandwich structure, where the thickness of the Cu overlayer is over 100 nm (1-6). It is hard to characterize the interfacial interactions that govern the adhesion, diffusion and nucleation of Cu on these potential diffusion barriers at such length scales. A detailed understanding of the nature of the Cu/barrier interface is of technological importance to determine optimum barrier layer surface chemistry and processing for Cu wetting, adhesion and interfacial stability. Studies on the growth mode and ultrathin (< 50 Å) overlayers of Cu on Ta(110) (7), W(110) (8-11), W(100) (12) as well as TiO_2(110) (13) have been reported. Such studies focus on the interaction of Cu with typically idealized single crystal surfaces where the effect of impurities is neglected. Surface studies on polycrystalline substrates, where grain boundary diffusion of Cu is dominant (14), are rare. The work involved in this chapter focuses on the effect of impurities (O, C) on the wetting/de-wetting behavior as well as diffusion kinetics of Cu on polycrystalline Ta. Auger electron spectrocsopy (AES) and temperature programmed

desorption (TPD) results under ultra high vacuum (UHV) conditions point to the importance of sub-monolayer surface coverages of impurities in controlling the wetting and diffusion behavior of Cu.

Cu thermal diffusion into polycrystalline barriers is dominated by grain boundary diffusion (14). Improvements of barrier performance have been achieved by intentionally contaminating bulk barrier materials with impurity atoms (O, C, N, etc.) (2, 15-17). It is believed that these impurities segregate to the grain boundaries and defects, resulting in the blockage of those diffusion pathways.

Recent research (6) indicates that an amorphous interfacial layer with a thickness of about 50 Å is formed by annealing the Cu/Ta(002) interface at 673 K, despite predictions based on the solid state phase diagram that Cu and Ta are immiscible (18). This interfacial mixing greatly affects the adhesion/diffusion characteristics of Cu on barrier materials. The interfacial thickness (~ 50 Å) implies that the ultra-thin barriers required for future devices may be readily compromised by such phenomena. The TPD results from this work support the formation of such an interfacial layer.

The studies presented in this chapter show that even a sub-monolayer of oxygen on Ta drastically reduces the ability of Cu to wet the surface upon heating, as does an overlayer of TaC. A surprising result is that the kinetics of Cu diffusion into the substrate are affected by sub-monolayer surface impurity concentrations. Oxygen and carbide adlayers retard the thermal diffusion of Cu into the bulk. Surface studies also indicate that a Cu-Ta mixed interphase forms during the annealing of Cu deposited on polycrystalline Ta in UHV. These results have significant implications for the “real

world" practices, where the presence of bulk and surface impurities is inevitable. The significance of these results for other refractory diffusion barriers (W, TaN, etc.) will also be discussed.

3.2. Experimental Methods

The experiments were performed in a UHV chamber equipped with AES and TPD capabilities (19). The schematic diagram of the chamber was shown in Figure 2.2. Typical working pressures in the chamber were $2\text{-}5 \times 10^{-10}$ Torr. The Ta sample consisted of polycrystalline foil (99.99%, 0.05 mm thick) about 1 cm^2 in area, and was attached to the manipulator by two Ta support leads. The sample temperature was monitored by a K-type thermocouple spot-welded to the back of the sample. The manipulator allowed resistive heating to 1500 K and liquid nitrogen cooling to 80 K. The surface was cleaned by cycles of Ar ion sputtering (2 KeV) and annealing to 1100 K. This procedure was sufficient to remove most of the surface impurities from Ta. The high solubility of oxygen in Ta, however, caused a diffusion of oxygen from the bulk to the surface upon annealing to elevated temperatures. Complete removal of carbon was also not accomplished because it would require heating to above 2000 K (20), which was not possible with this manipulator. The typical well-sputtered and annealed Ta surfaces used for the experiments had less than 10% coverages of oxygen and carbon each.

Gas dosing was performed by introducing gases (oxygen, 1,3-butadiene) through separate manual leak valves and directional doser tubes. Exposures were determined by monitoring background pressure in the chamber and time of exposure. Coverages are

reported here in Langmuir (1 L = 10^{-6} Torr-s) and have not been corrected for the effects of ion gauge sensitivity, or directional dosing. Oxidation of Ta was carried out with oxygen (99.997%) gas at room temperature. Surface carbide was formed by dosing 1,3-butadiene (99%wt minimum in liquid phase) at 90 K, followed by electron beam treatment (5 $\mu A/cm^2$, 10 min) (21) of the adsorbed butadiene layer and flash annealing to 1000 K. Carbide formation was evidenced by the characteristic carbon AES line shape (22).

Cu evaporation was performed with an evaporator that consisted of a Cu (99.95%, oxygen-free) ribbon wrapped around a W filament. Evaporation was conducted by controlling the heating current and the evaporation time. Filament temperature and Cu flux were not determined.

A linear heating rate of 10 K/s was used in TPD measurements. A quardrupole mass spectrometer was collimated for line-of-sight mass measurements. Up to ten different atomic mass unit (amu) channels can be acquired from a single run through a computer program.

AES spectra were collected in the differential mode using a cylindrical mirror analyzer, a lock-in amplifier (4 eV peak-to-peak modulation), and a X-Y recorder. The electron excitation energy was 3KeV. Relative concentrations of surface species were determined by using published Auger sensitivity factors (22) and peak-to-peak signal intensities according to

$$N_A/N_B = I_A X_B / I_B X_A \qquad (3\text{-}1)$$

Where N, I and X represent respectively, the atomic concentration, the peak-to-peak

intensity and the atomic sensitivity factor of a certain element. The thickness of an overlayer on Ta was calculated using the mean free path value of 7.2 Å (23) for the Ta(179eV) transition and the equation

$$I = I_0 \exp(-d/\lambda) \quad (3\text{-}2)$$

Where I_0 and I are the intensities of Ta signal before and after the overlayer deposition respectively, and d is the thickness of the overlayer, and λ the inelastic mean free path of Ta.

3.3. Results

3.3.1. Oxidation of Ta substrate at room temperature

An oxide surface layer was formed by exposing the Ta surface to O_2 at room temperature under UHV conditions. Figure 3.1 shows the change in relative oxygen coverage (O/Ta atomic ratio) as a function of O_2 exposure at 300 K. The concentration of oxygen on the surface increases initially with exposure until it reaches a saturation coverage at 10 L. At this coverage, an oxide overlayer thickness of 2.2 Å was calculated with the use of Equation (3-2). Since the ionic diameter of O is 2.8 Å (24), one can infer that a monolayer thick oxide overlayer is formed on the Ta surface upon exposing it to O_2 at room temperature. Himpsel et al. (25) have shown that O_2 exposures at relatively high oxygen pressures (10^{-6} Torr) and elevated temperatures (~1000 K) cause the growth of bulk oxides, whose much slower growth mechanism causes the rate of oxygen adsoption to decrease markedly. Under our experimental conditions (room temperature, low oxygen pressure of 1×10^{-8} Torr), the oxidation of the Ta substrate is unlikely to

proceed beyond the surface stage into bulk oxide formation. Similar behavior has been reported in previous studies on the oxidation of Ta (26, 27) and Nb (28-30). These studies have shown that small O_2 exposures at room temperature lead to chemisorbed atomic oxygen, followed by the formation of a monolayer thick surface oxide.

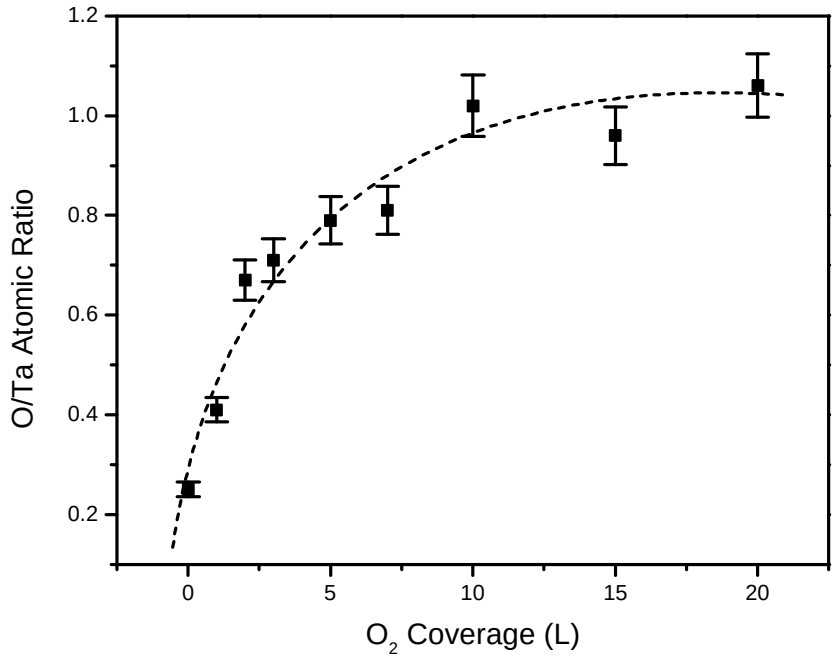

Figure 3.1. Relative O/Ta atomic ratio by AES versus O_2 exposure on Ta(poly) surface at 300 K.

3.3.2. Carbide formation on Ta substrate

A thin layer of tantalum carbide was formed by the surface reaction between the 1,3-butadiene and the Ta substrate with electron beam bombardment (5 $\mu A/cm^2$, 10 min) at 90 K and thermal annealing to 1000 K. The adsorption of 1,3-butadiene on Ta is negligible at room temperature under UHV conditions as evidenced by Auger spectra

taken after the exposure. Carbide overlayers on transition metal surfaces have been produced by the thermal cracking of unsaturated hydrocarbon molecules such as ethylene and 1,3-butadiene at temperatures above 600 K (31-33). In this study, the growth of a monolayer of carbide on the Ta surface was carried out at 90 K with the assistance of electron beam bombardment.

TPD spectra before (a) and after (b) treating the butadiene (0.1 L)/Ta sample with electron beam are displayed in Figure 3.2. The peak at ~170 K is shared by all the

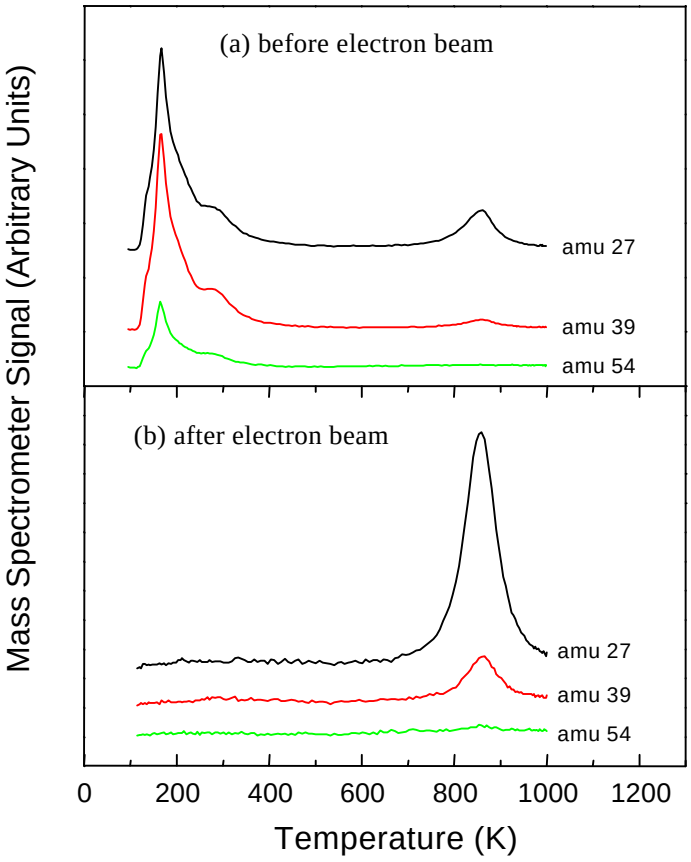

Figure 3.2. Desorption of 0.1 L 1,3-butadiene from a Ta(poly) surface at 90 K (a) before and (b) after electron beam bombardment (5 μA/cm^2, 10 min).

ionization fragments of 1,3-butadiene, which include $CH_2=CH^+$ (amu 27), $CH_2=CHC^+$ (amu 39) and $CH_2=CH-CH=CH_2^+$ (amu 54). This peak is attributed to the multilayer desorption of 1,3-butadiene. Given the low adsorption temperature and directional dosing, multilayer formation is not surprising. The second peak at ~280 K is most likely due to the molecular desorption from the first monolayer. The third peak at ~ 860 K is the result of surface decomposition and recombination reactions at elevated temperatures. The absence of the parent ion ($CH_2=CH-CH=CH_2^+$, amu 54) desorption at this temperature indicates that the 1,3-butadiene has reacted with the surface. The desorption behavior of 1,3-butadiene after subjecting it to electron beam bombardment (5 $\mu A/cm^2$, 10 min) is markedly different as shown in Figure 3.2(b). In this case both the molecular desorption features below 300 K are absent. The only desorption peak observed is that of the decomposition/ recombination products at 860 K. Subsequent thermal ramp (not shown) reveals that even the 860 K feature is absent, indicating that the only species that remained on the Ta surface after the second anneal was the carbide.

Direct evidence of carbide formation upon electron beam bombardment and TPD (thermal ramp) is demonstrated by the Auger spectra in Figure 3.3. A distinct change in the carbon Auger line shape can be observed before (a) and after (b) the thermal ramp. The split peaks near 252, 260 and 271 eV are the spectral signature of carbidic carbon species (22). The Auger spectrum collected after the thermal ramp for the butadiene/Ta sample without electron beam bombardment is also shown in Figure 3.3(c). It is evident from these spectra that the electron beam bombardment followed by thermal annealing results in the carbide formation. Calculations using Equation (3-1) and (3-2) reveal that

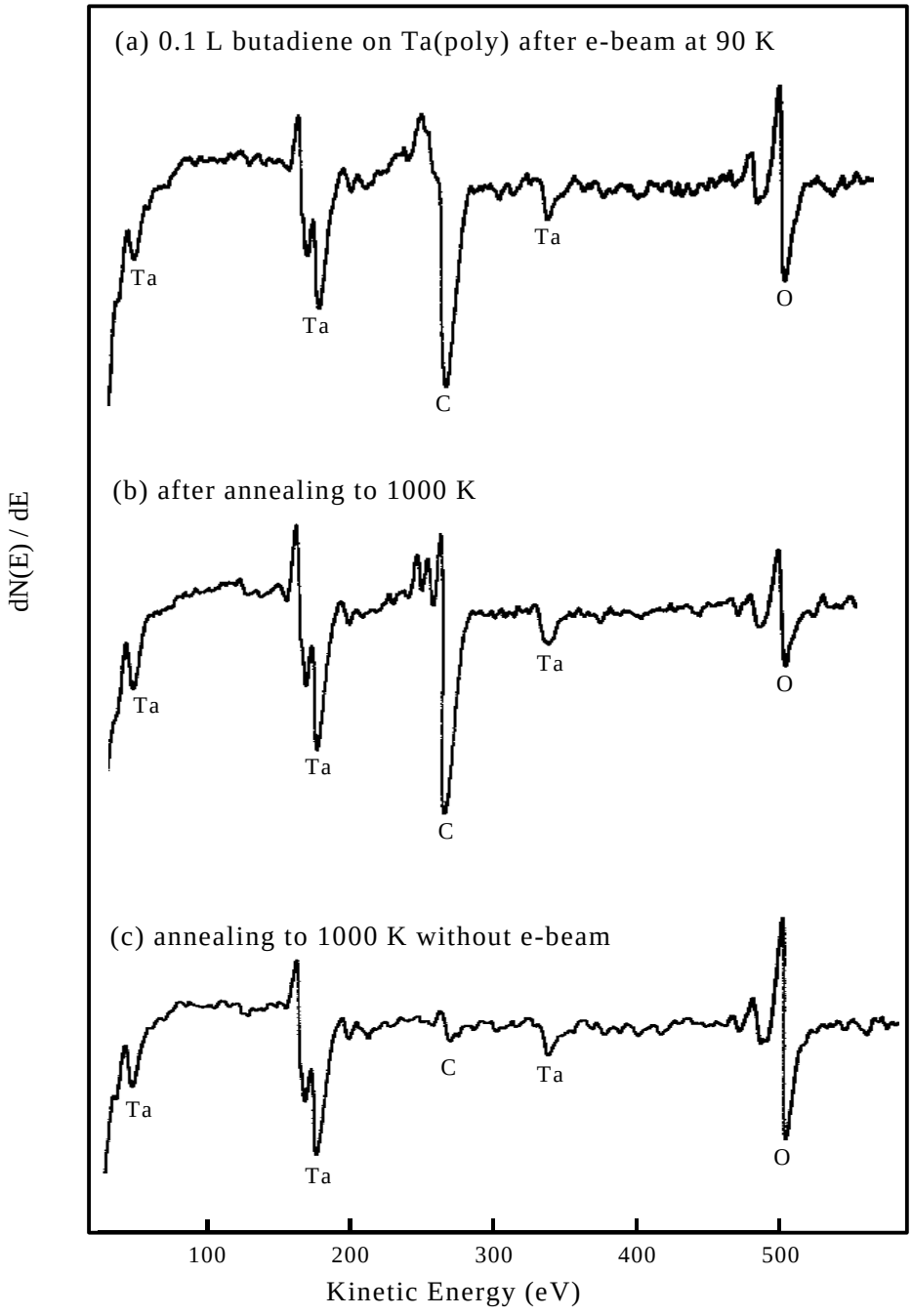

Figure 3.3. Auger spectra of a Ta(poly) surface exposed to 0.1 L 1,3-butadiene followed by electron beam bombardment (5 $\mu A/cm^2$, 10 min) at 90 K (a) before and (b) after a thermal ramp to 1000 K (TPD); (c) the same surface annealed to 1000 K without electron beam bombardment.

the carbides formed by this method have an average C/Ta atomic ratio of 1.1 ± 0.1, which corresponds to a carbide overlayer thickness of 3.5 ± 0.4Å.

3.3.3. Cu interaction with "clean" Ta(poly) substrates

In order to study the thermal stability of Cu overlayer on Ta substrates, thin layers of Cu with various thicknesses were deposited on a clean Ta surface at 300 K and the sample was annealed to progressively higher temperatures (10 min at each temperature). The Cu/Ta sample was then cooled down to 300-400 K to allow for AES measurements. The Cu(920 eV)/Ta(179 eV) atomic ratio and Cu(920 eV)/Cu(60 eV) peak-to-peak intensity ratio are presented as a function of temperature in Figure 3.4 for different initial Cu coverages. The variation in the Cu(920 eV)/Ta(179 eV) atomic ratio reflects the change of Cu surface concentration. This variation, however, does not discriminate between diffusion and surface nucleation (de-wetting), because both of these processes lead to a decrease in the Cu/Ta Auger intensity ratio. The Cu(920 eV)/Cu(60 eV) peak-to-peak intensity ratio, on the other hand, allows one to determine whether diffusion or de-wetting has taken place. Due to the different mean free paths of these two Auger transitions (18 Å at 920 eV and 4 Å at 60 eV (23)), the Cu(60 eV) signal is more surface sensitive. While surface nucleation causes little change to the Cu(920 eV)/Cu(60 eV) ratio, Cu diffusion into the bulk causes the ratio to increase (34).

For a 2 Å Cu overlayer (Figure 3.4(a)), annealing to 1000 K results in no significant change in the Cu/Ta intensity ratio. The surface concentration of Cu remains fairly stable until 1000 K; above 1000 K it decreases rapidly.

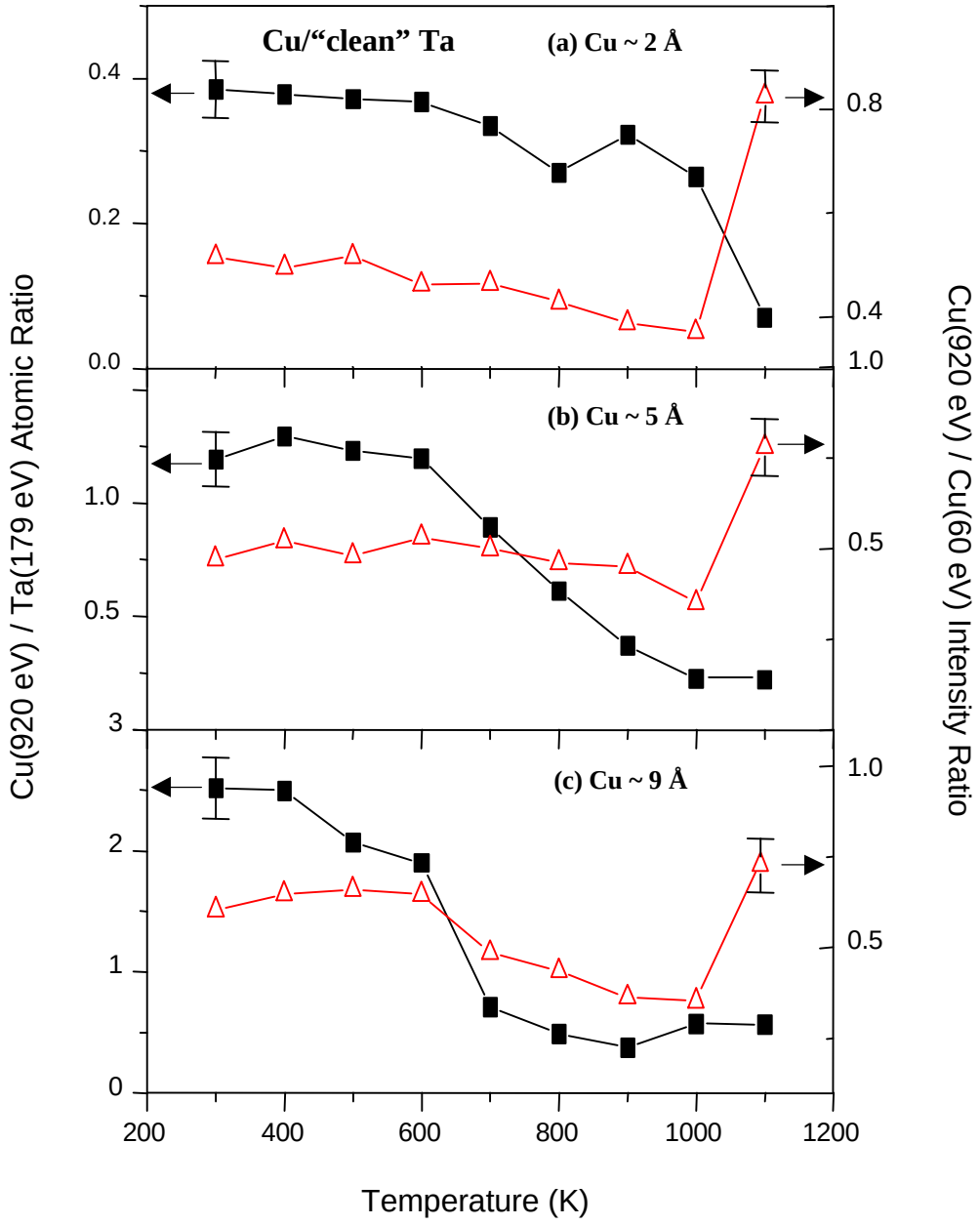

Figure 3.4. AES ratios as a function of temperature for Cu overlayer on a clean Ta(poly) substrate. Cu initial coverage at 300 K was (a) 2 Å, (b) 5 Å, and (c) 9 Å respectively.

The corresponding Cu(920 eV)/Cu(60 eV) ratio exhibits a similarly stable temperature range below 1000 K, followed by a pronounced increase at 1100 K. This indicates that for ultrathin Cu films (less than one monolayer, considering the 1.40 Å van der Waals radius of Cu (35)), the Cu does not de-wet Ta upon heating. It remains relatively stable till 1000 K, at which temperature diffusion into the bulk occurs.

A distinctly different behavior can be observed when the Cu coverage is increased to 5 Å (Figure 3.4(b)). The Cu/Ta ratio remains stable during annealing of the Cu films from 300 K to 600 K. Upon heating the sample from 700 K to 1000 K, the Cu/Ta Auger intensity ratio decreases consistently. During this period, the Cu(920 eV)/Cu(60 eV) Auger intensity ratio reveals that diffusion of Cu into the bulk is not happening. Hence, the decrease in the Cu/Ta intensity ratio in the 600 K to 1000 K region is attributed to Cu surface nucleation. Figure 3.4(b) also demonstrates that Cu diffusion into the bulk becomes appreciable at 1100 K. A similar result is obtained when the Cu coverage is increased to 9 Å as shown in Figure 3.4(c). Significant decrease in the Cu/Ta ratio is observed above 600 K. This, together with the trend in the Cu(920 eV)/Cu(60 eV) ratio, indicates that the 9 Å Cu film also de-wets the Ta substrate at 600 K. The nucleation process, however, is accomplished in much shorter period (600-700 K) than in the 5 Å Cu film (600-1000 K). In all three cases diffusion of Cu into the bulk was observed only at 1100 K.

3.3.4. Cu de-wetting behavior on oxygen covered Ta(poly) substrates

The effect of surface oxidation on the de-wetting/diffusion behavior of Cu was studied by depositing 5 Å of Cu on oxygen covered Ta substrates, followed by annealing.

The results of various oxygen coverages are compared to “clean” Ta in Figure 3.5.

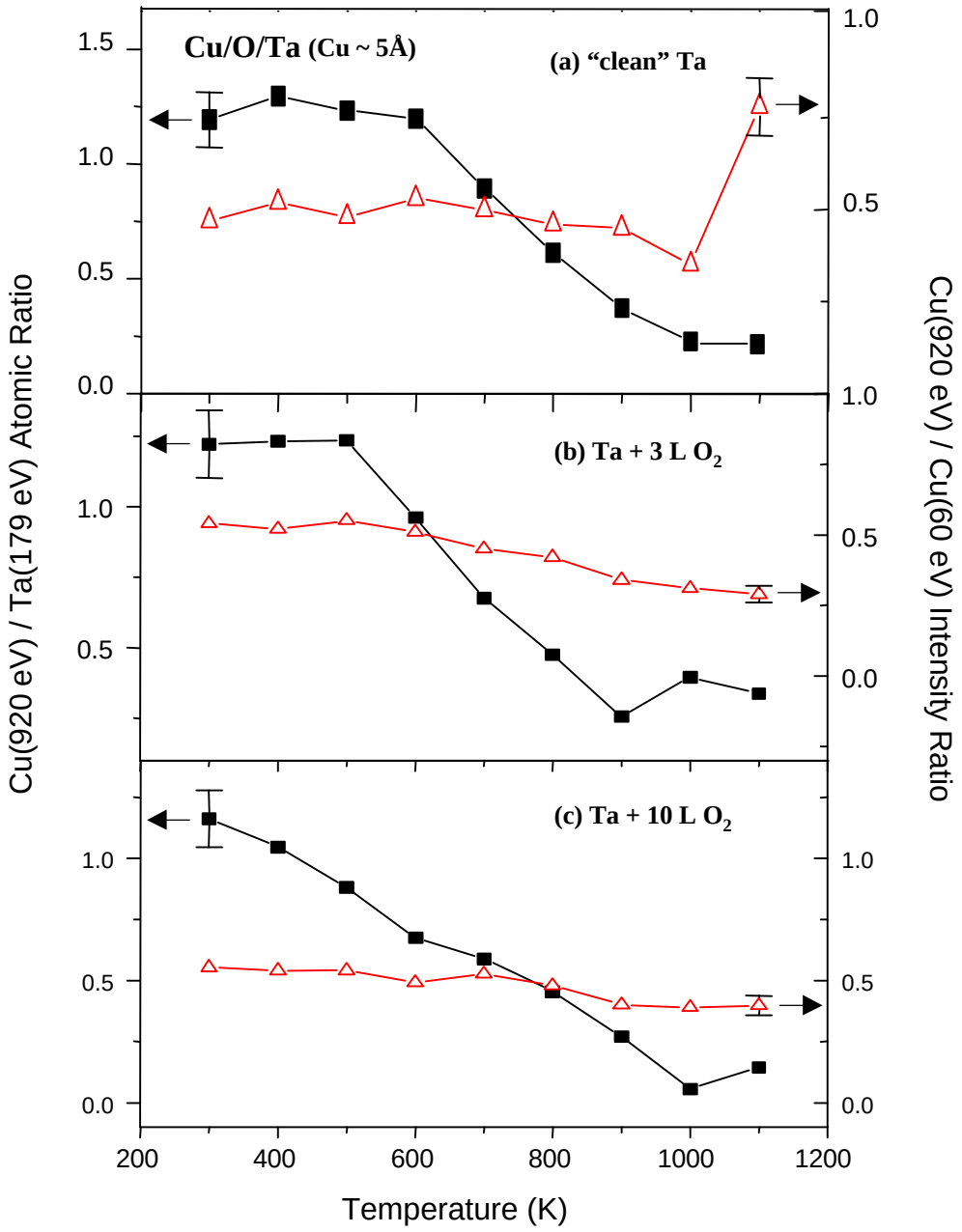

Figure 3.5. The effect of oxygen coverage on the thermal stability of a Cu/O/Ta(poly) layer. Cu coverage was 5 Å. Oxygen pre-dosage was (a) zero, (b) 3 L, and (c) 10 L respectively.

For a 3 L O_2 exposure the oxygen coverage is equivalent to 0.7 monolayer (Figure 3.1). Figure 5(b) shows that the Cu/Ta ratio starts to decrease at 500 K. Since the Cu(920 eV)/Cu(60 eV) ratio does not change at this temperature, the decrease in Cu/Ta intensity is caused by the nucleation of the Cu overlayer on the surface. A more pronounced effect is obtained at one monolayer oxygen coverage (10 L O_2), which further lowers the Cu de-wetting temperature to 300 K. Cu diffusion was not detected for oxygen covered Ta substrates under these annealing conditions (10 min at each temperature). This implies that surface oxidation affects both de-wetting and diffusion behaviors of Cu overlayer upon thermal annealing.

In order to clarify the role of surface oxygen on the de-wetting behavior of Cu overlayer, corresponding O/Ta atomic ratios are plotted as a function of temperature in Figure 3.6. The change in oxygen content upon heating follows exactly the same pattern as that of the Cu/Ta ratio. Namely, significant decrease in the O/Ta ratio occurs at 600, 500 and 300 K, respectively, for "clean", 3 L and 7 L O_2-covered Ta surface. This suggests that the surface O undergoes a concurrent nucleation process with Cu upon annealing. In the absence of Cu, the change in the O/Ta ratio for a sputter-cleaned Ta sample (plotted in dotted line) is negligible upon heating. This indicates that the decrease in O content is specifically due to the interaction of O with Cu. Similar repulsion induced phase separation between Cu and O atoms has been previously reported by Gomer and co-workers for Cu films deposited on a chemisorbed-oxygen-covered W(110) surface (8, 10).

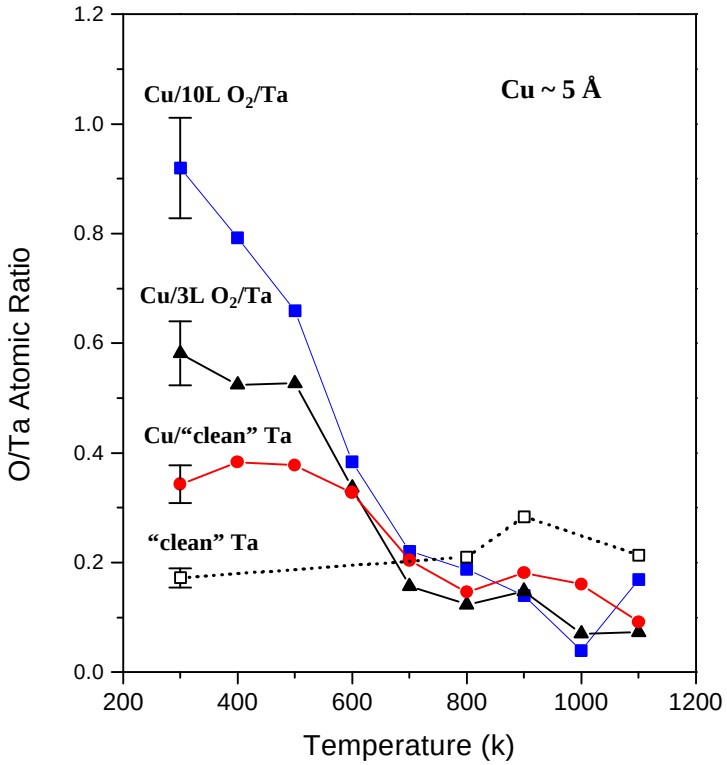

Figure 3.6. The change of oxygen surface concentration with annealing temperature for a Cu/O/Ta(poly) layer with different oxygen coverage. Cu coverage was 5 Å. The relative O/Ta atomic ratio of a "clean" Ta is presented in dotted line for comparison.

3.3.5. Cu de-wetting behavior on carbidic Ta(poly) substrate

Carbide formation on Ta can also dramatically change the wetting/de-wetting behavior of Cu as demonstrated in Figure 3.7. The de-wetting temperature of Cu (5 Å) occurs also at 300 K as indicated by the sharp decrease of Cu/Ta intensity ratio. Since the Cu(920 eV)/Cu(60 eV) ratio stays relatively stable over the whole temperature range, it is

inferred that the decline in the Cu/Ta intensity ratio is not caused by diffusion.

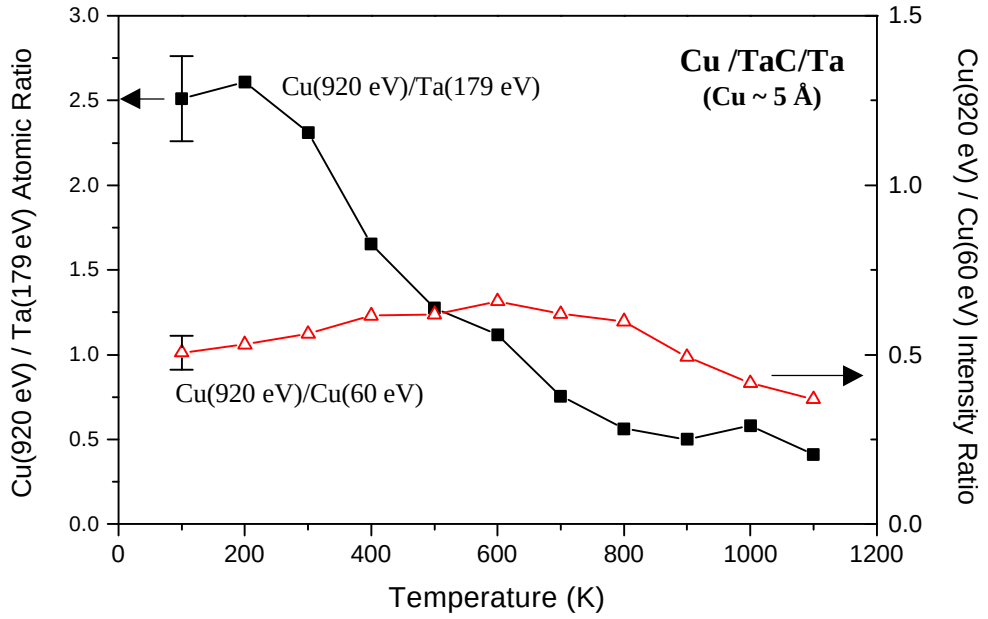

Figure 3.7. AES ratios as a function of temperature for Cu overlayer on a carbide covered Ta(poly) substrate. Cu initial coverage was 5 Å at 100 K.

The changes in C (from carbide) and O (internal impurity) relative intensity during thermal annealing with or without the Cu overlayer are presented in Figure 3.8. In the absence of Cu overlayer in Figure 3.8(a), C and O intensity remain roughly constant till 900 K. Above 900 K, the relative C intensity decreases substantially while no significant change is detected for the O concentration. In the presence of 5 Å Cu in Figure 3.8(b), a similar trend is observed for C except that this time the decrease occurs at 800 K. However, a strikingly different behavior is observed for O. The O intensity starts to decrease at 400 K. This is attributed to the strong repulsion between Cu and oxide, which

induces the formation of separate Cu and O domains (8, 10).

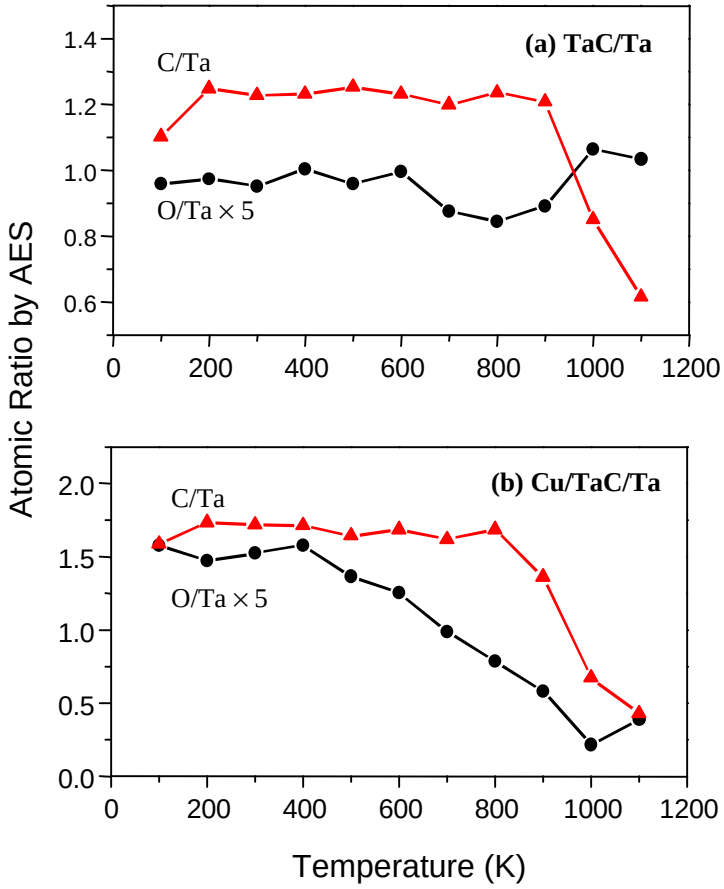

Figure 3.8. The change of carbon and oxygen surface concentration with annealing temperature for a (a) TaC/Ta, and (b) Cu/TaC/Ta layer.

3.3.6. Cu diffusion kinetics on "clean", oxidized and carbidic Ta(poly) substrates

The above data indicate that Cu diffusion at 1100 K only occurs on clean Ta, under the employed annealing conditions (10 min at each temperature setting). However, under prolonged annealing at 1100 K, Cu diffusion was observed after different induction periods for oxygen and carbide modified Ta substrates. The diffusion of Cu as a function

of annealing time at 1100 K is show in Figure 3.9. The divergence of Cu(920 eV)/Cu(60 eV) AES ratio is indicative of Cu diffusion into the bulk. No desorption of Cu was observed at 1100 K from TPD (not shown), which is consistent with Cu diffusion rather than desorption. Cu diffusion does not occur for clean Ta until an incubation time of 5 min. This induction period was reproducible whether the sample was kept continuously at 1100 K or cycled between 1100 K and 400 K (when Auger measurements were taken). As long as the total annealing time at 1100 K did not exceed 5 min, no Cu diffusion was observed. Different induction times were also obtained for O and C modified Ta substrates. As shown in Figure 3.9, it requires 10 min for Cu diffusion to occur on partially oxidized Ta, 15 min on carbide covered Ta and 20 min on Ta with saturation oxygen coverage. This indicates that the kinetics of Cu diffusion in Ta are affected by surface impurity levels. Introduction of ~ monolayer concentrations of contaminant atoms (O, C) appears to retard the diffusion of Cu in Ta substrates. It should be point out that the annealing temperature, as well as the annealing time, is also a critical factor for the Cu diffusion process. Extended annealing was performed for the above systems at 600, 900 and 1000 K for up to 60 min. No Cu diffusion was observed at those temperatures.

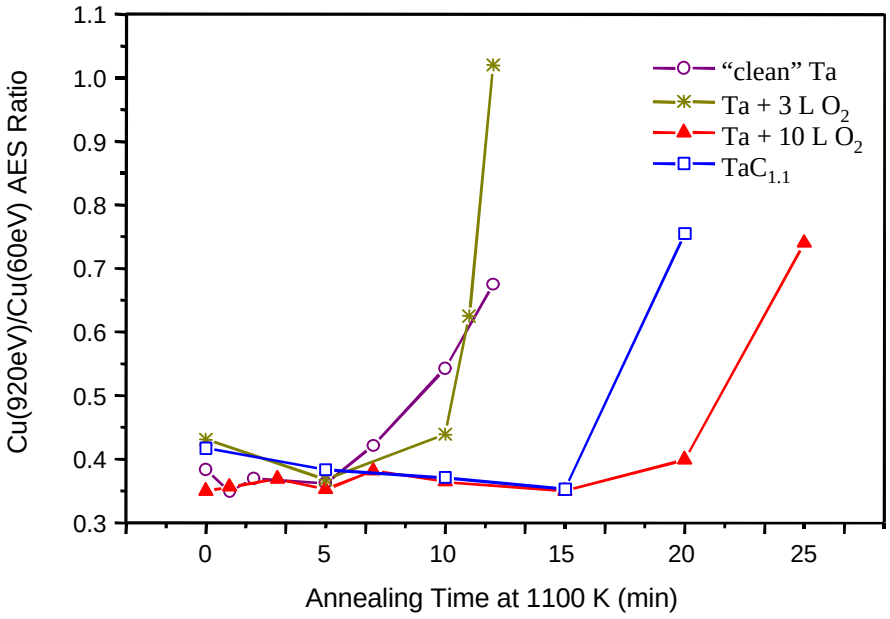

Figure 3.9. Cu(920eV)/Cu(60eV) AES ratio for clean and O, C modified Ta substrates versus annealing time at 1100 K. The increase in the ratio indicates Cu diffusion.

3.3.7. Cu desorption from "clean" Ta(poly)

TPD results for Cu multilayer on a "clean" Ta surface are shown in Figure 3.10. The Cu coverage is estimated 40 Å judging by the complete attenuation of Ta signal. A first anneal to 1200 K was carried out but no desorption of Cu (mass 63) was detected. Auger measurement after the first anneal indicated no change in Cu intensity. A second TPD was performed toward 1400 K. Due to the difficulty to maintain heating at temperatures above 1300 K, TPD experiments were terminated prematurely at 1350 K, causing the asymmetric shape of the desorption peak. As shown in Figure 3.10, one Cu desorption peak is observed at above 1300 K as opposed to the two TPD features due to monolayer and multilayer desorption of Cu on Ta(110) (see the insert in Figure 3.10 (7)).

The lack of multilayer desorption peak at lower temperature and the significantly higher desorption temperature (compared to the 1150 K sublimation temperature of Cu (9)) are evidence that the Cu is chemically bound to Ta. This corroborates results of Wong and co-workers (6) in indicating that Cu forms a pseudo-two dimensional mixing layer with Ta(002) substrates with a thickness of ~ 50 Å.

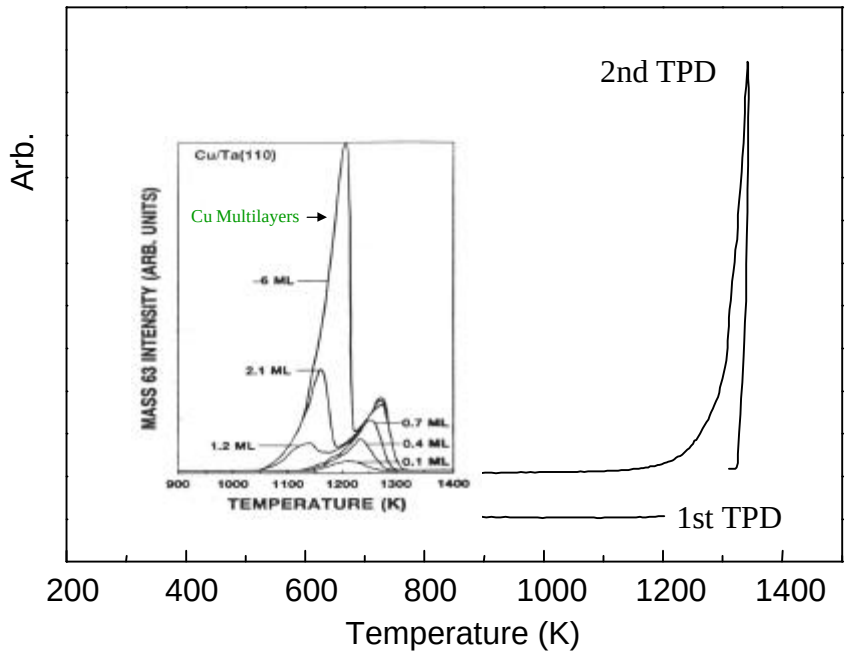

Figure 3.10. TPD spectra of Cu (mass 63) from a clean Ta(poly) surface. Cu initial coverage was ~ 40 Å at 300 K. First anneal was carried out to 1200 K, second 1350 K. The insert (7) shows the Cu TPD on a Ta(110) surface.

3.4. Discussions

Since the wetting/de-wetting of metal overlayers with substrates is well correlated with the work of adhesion (9), the wetting behavior of Cu on a substrate is not only of

practical significance during deposition, but also a guide to subsequent interfacial stability. For sub-monolayer (2 Å) coverage of Cu at room temperature, annealing to 1000 K does not cause Cu to de-wet "clean" Ta substrate (Figure 3.4a). This indicates that the Cu adatoms form a conformal first layer on Ta(poly) at room temperature. The formation of a "smooth" first layer of Cu has been observed by Goodman et al. on a Ta(110) surface (7). As evidenced by their TPD results (see insert in Figure 3.10), only one desorption feature is present for submonolayer coverages of Cu (vapor-deposited at ~350 K). For Cu coverages greater than one monolayer, a second peak develops at lower temperature. The second peak corresponds to multilayer desorption while the first to monolayer desorption. The existence of a conformal first layer indicates that the interaction between Cu-substrate is stronger than that of Cu-Cu. Such substrates include Ta(110) (7), W(110) (9, 36), W(100) (36), as well as Al_2O_3/Al(111) (34).

Annealing of 5 Å Cu overlayer on various Ta substrates result in the 3-D nucleation of Cu at elevated temperatures. The decrease in Cu Auger intensity on partially oxidized Ta substrates coincides with the decrease in O Auger intensity (Figure 3.5 and 3.6), indicating the segregation of Cu and O into separate domains. This phase separation, induced by strong Cu-O repulsion, has been reported on Cu/O_2/W(110) systems (8, 11). Contrasting behavior is observed for the Cu/Al_2O_3/Al(111) system (34), where Cu diffusion through the oxide layer occurs upon heating. This results in the concurrent decrease in Cu Auger intensity and increase of O intensity due to the diminished attenuation of the Al_2O_3/Al(111) substrate.

Unusual induction periods are observed for the thermal diffusion of Cu into

"clean" and modified Ta substrates (Figure 3.9). This cannot simply be attributed to the segregation of impurity atoms into grain boundaries, since the C and O coverages are at the monolayer range. One can hardly expect that such minor concentrations of impurity would effectively block the diffusion pathways of Cu. The fact that Cu diffusion occurs at the same temperature but after different retardation periods suggests that the mechanism is kinetically, rather than thermodynamically, driven. Unfortunately, the exact mechanism of this process cannot be elucidated by the experimental data collected so far.

Since barrier layers even in some present devices (e.g., near the corners of trenches) may approach 50 Å in thickness, the formation of such pseudo-two dimensional mixing layers presents a significant threat to the integrity of conventional diffusion barrier materials. Data from the literature (12) suggest that this mixing effect may occur on W as well as Ta surfaces. The data also suggest that this mixing effect may be extremely sensitive to surface structure, that is, it occurs only on (100) or similar surfaces (6, 12) but not on (110) surfaces (7, 36). Furthermore, such mixing may also be affected by the presence of impurities because impurities such as C, N and O prefer to occupy the high coordinate site at such surfaces (e.g., the 4-fold site on the (001) surface). Since Cu may also prefer such high coordinate sites (12), the implication is that impurity occupancy of high coordinate sites will critically affect Cu wetting, adhesion and diffusion at W and Ta-containing barrier layers. Therefore, even minor surface contamination encountered during cluster tool processing can significantly affect Cu/Ta interfacial properties. This has significant implications for the type of pre-cleaning/contamination control required

for consistent interface properties.

3.5. Summary and Conclusions

The thermal stability of Cu on clean, oxidized, and carbidic Ta substrates was studied under UHV conditions with the use of Auger electron spectroscopy. Analysis of the intensity ratios between Cu/Ta and Cu/Cu shows that even sub-monolayer coverages of oxygen or carbide on polycrystalline Ta significantly degrade the strength of Cu/Ta chemical interactions. Surface nucleation of Cu on clean Ta substrates occurs above 600 K. The presence of 0.7 monolayer of oxygen on Ta samples, however, lowers this de-wetting temperature to 500 K. The de-wetting temperature is further lowered to 300 K when the Ta substrate is pre-covered with a monolayer of oxygen. Similar behavior was observed for Ta substrates modified by carbide. Cu starts to de-wet C/Ta surface at monolayer coverages of carbide above 300 K. The diffusion of Cu into the bulk Ta is similarly affected by oxygen and carbon. If the surface temperature of the clean Ta is held at 1100 K, Cu diffuses into the bulk after an induction period of 5 min. This induction period increases to 10 min for partially oxidized Ta, 15 min for carbidic Ta and 20 min for fully oxidized Ta. It is clear from these results that the diffusion barrier property of polycrystalline Ta improves with the incorporation of impurity atoms. This improvement, however, comes at the expense of weakened Cu adhesion on Ta as demonstrated by reduction of de-wetting temperature.

3.6. Chapter References

(1) Hu, C.-K.; Chang, S.; Small, M. B.; Lewis, J. E. *Proceedings of the International VLSI Multilevel Interconnection Conference* **1986**, 181-187.

(2) Clevenger, L. A.; Bojarczuk, N. A.; Holloway, K.; Harper, J. M. E.; C Cabral, J.; Schad, R. G.; Cardone, F.; Stolt, L. *J. Appl. Phys.* **1993,** *73*, 300.

(3) Olowolafe, J. O.; Mogab, C. J.; Gregory, R. B. *Thin Solid Films* **1993,** *227*, 37-43.

(4) Ono, H.; Nakano, T.; Ohta, T. *Appl. Phys. Lett.* **1994,** *64*, 1511.

(5) Jang, S.-Y.; Lee, S.-M.; Baik, H.-K. *J. Mater. Sci.: Mater. Electronics* **1996,** *7*, 271-278.

(6) Wong, S. S.; Ryu, C.; Lee, H.; Kwon, K.-W. *Mater. Res. Soc. Symp. Proc.* **1998,** *514*, 75.

(7) Kuhn, W. K.; Campbell, R. A.; Goodman, D. W. *J. Phys. Chem.* **1993,** *97*, 446-453.

(8) Lin, J. C.; Shamir, N.; Gomer, R. *Surf. Sci.* **1988,** *206*, 61-85.

(9) Peden, C. H. F.; Kidd, K. B.; Shinn, N. D. *J. Vac. Sci. Technol. A* **1991,** *9*, 1518.

(10) Shamir, N.; Lin, J. C.; Gomer, R. *J. Chem. Phys.* **1989,** *90*, 5135.

(11) Xu, H.; Yang, Y.-w.; Engel, T. *Surf. Sci. Lett.* **1992,** *275*, L707-L710.

(12) Hu, P.; Wander, A.; Garza, L. M. d. l.; Bessent, M. P.; King, D. A. *Surf. Sci. Lett.* **1993,** *286*, L542-546.

(13) Diebold, U.; Pan, J.-M.; Madey, T. E. *Phys. Rev. B* **1993,** *47*, 3868.

(14) Gupta, D. *Mater. Chem. Phys.* **1995,** *41*, 199-205.

(15) Ono, H.; Nakano, T.; Ohta, T. *Jpn. J. Appl. Phys. Part 1* **1995,** *34*, 1827-1830.

(16) Stavrev, M.; Fischer, D.; Preub, A.; Wenzel, C.; Mattern, N. *Microelectronic Eng.* **1997,** *33*, 269-275.

(17) Wang, W.; Booske, J. H.; Liu, H. L.; Gearhart, S. S.; Shohet, J. L.; Bedell, S.; Lanford, W. *J. Mater. Res.* **1998,** *13*, 726.

(18) Li, J.; Shacham-Diamond, Y.; Mayer, J. W. *Mater. Sci. Rep.* **1992,** *9*, 1-51.

(19) Chen, L.; Ekstrom, B.; Kelber, J. *Mater. Res. Soc. Symp. Proc.* **1999,** *564*, in press.

(20) Musket, R. G.; McLean, W.; Colmenares, C. A.; Makowiecki, D. M.; Siekhaus, W. J. *Appl. Surf. Sci.* **1982,** *10*, 143-207.

(21) Chen, L.; Kelber, J. A. *J. Vac. Sci. Technol. A.* **1999,** *17*, 1968.

(22) Davis, L. E.; MacDonald, N. C.; Palmberg, P. W.; Riach, G. E.; Weber, R. E. *Handbook of Auger Electron Spectroscopy*, Second ed.; Physical Electronics Industry, Inc.: Eden Prairie, Minnesota, 1976.

(23) Somorjai, G. A. *Introduction to Surface Chemistry and Catalysis*; John Wiley & Sons, Inc., 1994.

(24) Lide, D. R. *CRC Handbook of Chemistry and Physics*, 74th ed.; CRC Press, Inc., 1993.

(25) Himpsel, F. J.; Morar, J. F.; McFeely, F. R.; Pollak, R. A.; Hollinger, G. *Phys. Rev. B* **1984,** *30*, 7236.

(26) Veen, J. F. v. d.; Himpsel, F. J.; Eastman, D. E. *Phys. Rev. B* **1982,** *25*, 7388.

(27) Ruckman, M. W.; Qiu, S.-L.; Strongin, M. *Appl. Surf. Sci.* **1995,** *89*, 401-409.

(28) Dawson, P. H.; Tam, W.-C. *Surf. Sci.* **1979,** *81*, 464-478.

(29) Lindau, I.; Spicer, W. E. *J. Appl. Phys.* **1974,** *45*, 3720.

(30) Farrell, H. H.; Isaacs, H. S.; Strongin, M. *Surf. Sci.* **1973,** *38*.

(31) Chen, J. G.; DeVries, B. D.; Fruhberger, B.; Kim, C. M.; Liu, Z.-M. *J. Vac. Sci. Technol. A* **1995,** *13*, 1600.

(32) Chen, J. G.; Fruhberger, B.; Jr., J. E.; Bent, B. E. *J. Mol. Catal. A* **1998,** *131*, 285-299.

(33) Fruhberger, B.; Chen, J. G. *Surf. Sci.* **1995,** *342*, 38-46.

(34) Chen, J. G.; Colaianni, M. L.; Weinberg, W. H.; J T Yates, J. *Surf. Sci.* **1992,** *279*, 223-232.

(35) Huheey, J. E.; Keiter, E. A.; Keiter, R. L. *Inorganic Chemistry: Principles of Structure and Reactivity*, Fourth Edition ed.; HarperCollins College Publishers, 1993.

(36) Bauer, E.; Poppa, H.; Todd, G.; Bonczek, F. *J. Appl. Phys.* **1974,** *45*, 5164.

REFERENCES

MRS Bull. **1997,** *22*.

The National Technology Roadmap for Semiconductors: Technology Needs; Semiconductor Industry Association: San Jose, CA, 1997.

"http://www.chips.ibm.com/gallery/p-cw2.html".

Bauer, E.; Poppa, H.; Todd, G.; Bonczek, F. *J. Appl. Phys.* **1974,** *45*, 5164.

Berti, A.; Murarka, S. P. *Mater. Res. Soc. Symp. Proc.* **1994,** *318*, 451.

Bhattacharya, A. K. *J. Mol. Catal.* **1994,** *99*, 181.

Briggs, D.; Seah, M. P. Practical Surface Analysis. In *Practical Surface Analysis*; John Wiley & Sons Ltd, 1990; Vol. 1.

Case, C.; Kohl, P.; Kikkawa, T.; Lee, W. W. Low-Dielectric Constant Materials III; Mater. Res. Soc. Symp. Proc., 1997; Vol. 476.

Chang, C.-A.; Yee, D. S.; Petkie, R. *Appl. Phys. Lett.* **1989,** *54*, 2545.

Chang, K.-M.; Yeh, T.-H.; Deng, I.-C.; Shih, C.-W. *J. Appl. Phys.* **1997,** *82*, 1469.

Chen, J. G.; Colaianni, M. L.; Weinberg, W. H.; J T Yates, J. *Surf. Sci.* **1992,** *279*, 223-232.

Chen, J. G.; DeVries, B. D.; Fruhberger, B.; Kim, C. M.; Liu, Z.-M. *J. Vac. Sci. Technol. A* **1995,** *13*, 1600.

Chen, J. G.; Fruhberger, B.; Jr., J. E.; Bent, B. E. *J. Mol. Catal. A* **1998,** *131*, 285-299.

Chen, L.; Ekstrom, B.; Kelber, J. *Mater. Res. Soc. Symp. Proc.* **1999,** *564*, in press.

Chen, L.; Kelber, J. A. “polymerization of C-Si films on metal substrates: potential adhesion/diffusion barriers for microelectronics”; MRS Spring Meeting, 1998, San Francisco.

Chen, L.; Kelber, J. A. *J. Vac. Sci. Technol. A.* **1999,** *17*, 1968.

Chiang, C.; Ho, P. S.; Lu, T.-M.; Wetzel, J. T. Low-Dielectric Constant Materials IV; Mater. Res. Soc. Symp. Proc., 1998; Vol. 511.

Clevenger, L. A.; Bojarczuk, N. A.; Holloway, K.; Harper, J. M. E.; C Cabral, J.; Schad, R. G.; Cardone, F.; Stolt, L. *J. Appl. Phys.* **1993,** *73*, 300.

Davis, L. E.; MacDonald, N. C.; Palmberg, P. W.; Riach, G. E.; Weber, R. E. *Handbook of Auger Electron Spectroscopy*, Second ed.; Physical Electronics Industry, Inc.: Eden Prairie, Minnesota, 1976.

Dawson, P. H.; Tam, W.-C. *Surf. Sci.* **1979,** *81*, 464-478.

Diebold, U.; Pan, J.-M.; Madey, T. E. *Phys. Rev. B* **1993,** *47*, 3868.

Du, M.; Opila, R. L.; Case, C. *J. Vac. Sci. Technol. A* **1998,** *16*, 155.

Du, M.; Opila, R. L.; Donnelly, V. M.; Sapjeta, J.; Boone, T. *J Appl. Phys.* **1999,** *85*, 1496.

Endo, K. *MRS Bull.* **1997,** *22*, 55.

Endo, K.; Tatsumi, T. *J. Appl. Phys.* **1995,** *78*, 1370.

Endo, K.; Tatsumi, T. *Mat. Res. Soc. Symp. Proc.* **1995,** *381*, 249.

Endo, K.; Tatsumi, T. *Appl. Phys. Lett.* **1996,** *68*, 2864.

Endo, K.; Tatsumi, T. *Appl. Phys. Lett.* **1996,** *68*, 3656.

Endo, K.; Tatsumi, T. *Appl. Phys. Lett.* **1997,** *79*, 2616.

Endo, K.; Tatsumi, T.; Matsubara, Y. *Jpn. J. Appl. Phys.* **1996,** *35*, L 1348.

Ertl, G.; Kuppers, J. *Low Energy Electrons and Surface Chemistry*; VCH Publishers: New York, 1985.

Farrell, H. H.; Isaacs, H. S.; Strongin, M. *Surf. Sci.* **1973,** *38*.

Farrell, H. H.; Strongin, M. *Surf. Sci.* **1973,** *38*, 18-30.

Fink, D. G.; McKenzie, A. A. Electronics Engineer's Handbook; McGraw-Hill Book Company, 1975.

Fruhberger, B.; Chen, J. G. *Surf. Sci.* **1995,** *342*, 38-46.

Gamble, L.; Jung, L. S.; Campbell, C. T. *Langmuir* **1995,** *11*, 4505-4514.

Gaynor, J.; Ralston, A. *Semiconductor International* **1997,** *Dec.*, 73.

Grill, A.; Patel, V. *J. Appl. Phys.* **1999,** *85*, 3314.

Gupta, D. *Mater. Chem. Phys.* **1995,** *41*, 199-205.

Gutmann, R. J.; Chow, T. R.; Lakshminarayanan, S.; Price, D. T.; Steigerwald, J. M.; You, L.; Murarka, S. P. *Thin Solid Films* **1995,** *270*, 472-479.

Hacker, N. P. *MRS Bull.* **1997,** *22*, 33.

Han, L. M.; Timmons, R. B.; Lee, W. W.; Chen, Y.; Hu, Z. *J. Appl. Phys.* **1998,** *84*, 439.

Himpsel, F. J.; Morar, J. F.; McFeely, F. R.; Pollak, R. A.; Hollinger, G. *Phys. Rev. B* **1984,** *30*, 7236.

Holloway, K.; fryer, P. M.; Jr, C. C.; Harper, J. M. E.; Bailey, P. J.; Kelleher, K. H. *J. Appl. Phys.* **1992,** *71*, 5433.

Homma, T. *Mater. Sci. Eng.* **1998,** *R23*, 243-285.

Hu, C.-K.; Chang, S.; Small, M. B.; Lewis, J. E. *Proceedings of the International VLSI Multilevel Interconnection Conference* **1986**, 181-187.

Hu, P.; Wander, A.; Garza, L. M. d. l.; Bessent, M. P.; King, D. A. *Surf. Sci. Lett.* **1993,** *286*, L542-546.

Huheey, J. E.; Keiter, E. A.; Keiter, R. L. *Inorganic Chemistry: Principles of Structure and Reactivity*, Fourth Edition ed.; HarperCollins College Publishers, 1993.

Imahori, J.; Oku, T.; Murakami, M. *Thin Solid Films* **1997,** *301*, 142-148.

Jang, S.-Y.; Lee, S.-M.; Baik, H.-K. *J. Mater. Sci.: Mater. Electronics* **1996,** *7*, 271-278.

Jeng, S.-P.; Havemann, R. H.; Chang, M.-C. *Mat. Res. Soc. Symp. Proc* **1994,** *337*, 25.

Jeng, S.-P.; Taylor, K.; Chang, M.-C.; Ting, L.; Lee, C.; McAnally, P.; Seha, T.; Numata, K.; Tanaka, T.; Havemann, R. H. *Mat. Res. Soc. Symp. Proc.* **1995,** *381*, 197.

Jennison, D. R.; Kelber, J. A.; Rye, R. R. *Phys. Rev. B* **1982,** *25*, 1384.

Jin, C.; Luttmer, J. D.; Smith, D. M.; Ramos, T. A. *MRS Bull.* **1997,** *22*, 39.

Kaloyeros, A. E.; Chen, X.; Stark, T.; Kumar, K.; Seo, S.; Peterson, G. G.; Frisch, H. L.; Arkles, B.; Sullivan, J. *J Electrochem. Soc* **1999,** *146*, 170-176.

Kim, D. J.; Kim, Y. T.; Park, J.-W. *J. Appl. Phys.* **1997,** *82*, 4847.

Kolawa, E.; Pokela, P. J.; Reid, J. S.; Chen, J. S.; Nicolet, M.-A. *Appl. Surf. Sci.* **1991,** *53*, 373-376.

Kudo, H.; Shinohara, R.; Yamada, M. *Mat. Res. Soc. Symp. Proc.* **1995,** *381*, 105.

Kuhn, W. K.; Campbell, R. A.; Goodman, D. W. *J. Phys. Chem.* **1993,** *97*, 446-453.

Kurth, D. G.; Bein, T. *J. Phys. Chem.* **1992,** *96*, 6707-6712.

Kurth, D. G.; Bein, T. *Langmuir* **1995,** *11*, 578-584.

Kwak, J. S.; Baik, H. K.; Kim, J.-H.; Lee, S.-M. *Appl. Phys. Lett.* **1998,** *72*, 2832.

Kwon, K.-W.; Lee, H.-J.; Ryu, C.; Sinclair, R.; Wong, S. S. *Advanced Metallization and Interconnect Systems for ULSI Applications; Conference Proceedings* **1997**, 711-716.

Kwon, K.-W.; Ryu, C.; Sinclair, R.; Wong, S. S. *Appl. Phys. Lett.* **1997,** *71*, 3069.

Lacerda, M. M.; Jr, F. L. F.; Esteves, J. H. C. R.; Achete, C. A. *J. Phys. D: Appl. Phys.* **1997,** *30*, 944.

Lagendijk, A.; Treichel, H.; Uram, K. J.; Jones, A. C. Low-Dielectric Constant Materials II; Mater. Res. Soc. Symp. Proc., 1996; Vol. 443.

Lanford, W. A.; Ding, P. J.; Wang, W.; Hymes, S.; Murarka, S. P. *Mater. Chem. Phys.* **1995,** *41*, 192-198.

Lee, W. W.; Ho, P. S. *MRS Bull.* **1997,** *22*, 19.

Lee, Y.-J.; Suh, B.-S.; Kwon, M. S.; Park, C.-O. *J. Appl. Phys.* **1999,** *85*, 1927.

Li, J.; Shacham-Diamond, Y.; Mayer, J. W. *Mater. Sci. Rep.* **1992,** *9*, 1-51.

Li, J.; Strane, J. W.; Russell, S. W.; Hong, S. Q.; Mayer, J. W.; Marais, T. K.; Theron, C. C.; Pretorius, R. *J. Appl. Phys.* **1992,** *72*, 2810.

Lide, D. R. *CRC Handbook of Chemistry and Physics*, 74th ed.; CRC Press, Inc., 1993.

Limb, S. J.; Labelle, C. B.; Gleason, K. K.; Edell, D. J.; Gleason, E. F. *Appl. Phys. Lett.* **1996,** *68*, 2810.

Lin, J. C.; Shamir, N.; Gomer, R. *Surf. Sci.* **1988,** *206*, 61-85.

Lin, J.-C.; Lee, C. *Electrochem. Solid-State Lett.* **1999,** *2*, 181-183.

Lindau, I.; Spicer, W. E. *J. Appl. Phys.* **1974,** *45*, 3720.

List, R. S.; Singh, A.; Ralston, A.; Dixit, G. *MRS Bull.* **1997,** *22*, 61.

Liu, P. T.; Chang, T. C.; Sze, S. M.; Pan, F. M.; Mei, Y. J.; Wu, W. F.; Tsai, M. S.; Dai, B. T.; Chang, C. Y.; Shih, F. Y.; Huang, H. D. *Thin Solid Films* **1998,** *332*, 345-350.

Loke, A. L. S.; Ryu, C.; Yue, C. P.; Cho, J. S. H.; Wong, S. S. *IEEE Electron Device Lett.* **1996,** *17*, 549.

Lu, T.-M.; Moore, J. A. *MRS Bull.* **1997,** *22*, 28.

Lu, T.-M.; Murarka, S. P.; Kuan, T.-S.; Ting, C. H. Low-Dielectric Constant Materials - Synthesis and Applications in Microelectronics; Mater. Res. Soc. Symp. Proc., 1995; Vol. 381.

Ma, Y.; Yang, H.; Guo, J.; Sathe, C.; Agui, A.; Nordgren, J. *Appl. Phys. Lett.* **1998,** *72*, 3353.

Martini, D.; Kelber, J. A. **unpublished results**.

McBrayer, J. D.; Swanson, R. M.; Sigmon, T. W. *J. Electrochem. Soc.* **1986,** *133*, 1242.

Miller, R. D.; Hedrick, J. L.; Yoon, D. Y.; Cook, R. F.; Hummel, J. P. *MRS Bull.* **1997,** *22*, 44.

Mountsier, T. W.; Kumar, D. *Mat. Res. Soc. Symp. Proc.* **1997,** *443*, 41.

Muller, U.; Oral, R. H.; Tobler, M. *Surf. Coat. Technol.* **1995,** *76-77*, 367-371.

Murarka, S. P. *Solid State Technol.* **1996,** *39*, 83.

Murarka, S. P.; Gutmann, R. J.; Kaloyeros, A. E.; Lanford, W. A. *Thin Solid Films* **1993,** *236*, 257-266.

Murarka, S. P.; Hymes, S. W. *Crit. Rev. Solid State Mater. Sci.* **1995,** *20*, 87-124.

Musket, R. G.; McLean, W.; Colmenares, C. A.; Makowiecki, D. M.; Siekhaus, W. J. *Appl. Surf. Sci.* **1982,** *10*, 143-207.

Nix, R. *An Introduction to Surface Science*; http.//www.chem.qmw.ac.uk/surfaces/scc/sccinfo.htm, 1997.

Olowolafe, J. O.; Mogab, C. J.; Gregory, R. B. *Thin Solid Films* **1993,** *227*, 37-43.

Ono, H.; Nakano, T.; Ohta, T. *Appl. Phys. Lett.* **1994,** *64*, 1511.

Ono, H.; Nakano, T.; Ohta, T. *Jpn. J. Appl. Phys. Part 1* **1995,** *34*, 1827-1830.

Park, J. M.; Matienzo, L. J.; Spencer, D. F. *J. Adhersion Sci. Technol.* **1991,** *5*, 153.

Peden, C. H. F.; Kidd, K. B.; Shinn, N. D. *J. Vac. Sci. Technol. A* **1991,** *9*, 1518.

Raghavan, G.; Chiang, C.; Anders, P. B.; Tzeng, S.-M.; Villasol, R.; Bai, G.; Bohr, M.; Fraser, D. B. *Thin Solid Films* **1995,** *262*, 168.

Redhead, P. A. *Vacuum* **1962,** *12*, 203.

Reid, J. S.; Kolawa, E.; Ruiz, R. P.; Nicolet, M.-A. *Thin Solid Films* **1993,** *236*, 319-324.

Reid, J. S.; Lin, R. Y.; Smith, P. M.; Ruiz, R. P.; Nicolet, M.-A. *Thin Solid Films* **1995,** *262*, 218.

Ruckman, M. W.; Qiu, S.-L.; Strongin, M. *Appl. Surf. Sci.* **1995,** *89*, 401-409.

Runyan, W. R.; Bean, K. E. . In *Semiconductor Integrated Circuit Processing Technology*; Addison-Wesley Publishing Company: Reading, MA, 1990; pp. 518-578.

Runyan, W. R.; Bean, K. E. . In *Semiconductor Integrated Circuit Processing Technology*; Addison-Wesley Publishing Company: Reading, MA, 1990; pp. 124-126.

Ryan, E. T.; McKerrow, A. J.; Leu, J.; Ho, P. S. *MRS Bull.* **1997,** *22*, 49.

Sacher, E. *Prog. Surf. Sci.* **1994,** *4*, 273.

Senkevich, J. J.; Desu, S. B. *Appl. Phys. Lett* **1998,** *72*, 258.

Shacham-Diamond, Y.; Dubin, V. M. *Microelectronic. Eng.* **1997,** *33,* 47-58.

Shamir, N.; Lin, J. C.; Gomer, R. *J. Chem. Phys.* **1989,** *90*, 5135.

Simpson, J. O.; Clair, A. K. S. *Thin Solid Films* **1997,** *308-309,* 480-485.

Singer, P. *Semiconductor International* **1997,** *Nov.,* 67.

Singer, P. *Semiconductor International* **1998**, 42.

Somorjai, G. A. *Introduction to Surface Chemistry and Catalysis*; John Wiley & Sons, Inc., 1994.

Somorjai, G. A. *MRS Bull.* **1998,** *23,* 11.

Stavrev, M.; Fischer, D.; Preub, A.; Wenzel, C.; Mattern, N. *Microelectronic Eng.* **1997,** *33*, 269-275.

Sullivan, J. P.; Denison, D. R.; Barbour, J. C.; Newcomer, P. P.; Apblett, C. A.; Seager, C. H.; Baca, A. G. *Mat. Res. Soc. Symp. Proc.* **1997,** *443*, 149.

Sutcliffe, R.; Lee, W. W.; Gaynor, J. F.; Luttmer, J. D.; Martini, D.; Kelber, J.; Plano, M. A. *Appl. Surf. Sci.* **1998,** *126,* 43.

Theil, J. A.; Mertz, F.; Yairi, M.; Seaward, K.; Ray, G.; Kooi, G. *Mat. Res. Soc. Symp. Proc.* **1997,** *476,* 31.

Tillman, N.; Ulman, A.; Penner, T. L. *Langmuir* **1989,** *5*, 101-111.

Ting, C. H.; Seidel, T. E. *Mat. Res. Soc. Symp. Proc.* **1995,** *381,* 3.

Torres, J.; Mermer, J. L.; Madar, R.; Crean, G.; Gessner, T.; Bertz, A.; Hasse, W.; Plotner, M.; Binder, F.; Save, D. *Microelctronic Eng.* **1996,** *34*, 119-122.

Treichel, H.; Ruhl, G.; Ansmann, P.; Wurl, R.; Muller, c.; Dietlmeier, M. *Microelectronic Eng.* **1998,** *40,* 1-19.

Veen, J. F. v. d.; Himpsel, F. J.; Eastman, D. E. *Phys. Rev. B* **1982,** *25,* 7388.

Vogt, M.; Kachel, M.; Melzer, K.; Drescher, K. *Surf. Coat. Technol.* **1998,** *98*, 948.

Wang, M. T.; Lin, Y. C.; Chen, M. C. *J. Electrochem. Soc.* **1998,** *145,* 2538.

Wang, W.; Booske, J. H.; Liu, H. L.; Gearhart, S. S.; Shohet, J. L.; Bedell, S.; Lanford, W. *J. Mater. Res.* **1998,** *13*, 726.

Wasserman, S. R.; Tao, Y.-T.; Whitesides, G. M. *Langmuir* **1989,** *5*, 1074-1087.

Wiegand, B. C.; Lohokare, S. P.; Nuzzo, R. G. *J. Phys. Chem.* **1993,** *97*, 11553-11562.

Wong, S. S.; Ryu, C.; Lee, H.; Kwon, K.-W. *Mater. Res. Soc. Symp. Proc.* **1998,** *514*, 75.

Xu, H.; Yang, Y.-w.; Engel, T. *Surf. Sci. Lett.* **1992,** *275*, L707-L710.

Xu, J.; Choyke, W. J.; Yates, J. T. J. *Appl. Surf. Sci.* **1997,** *In Press.*

Yang, H.; Tweet, D. J.; Ma, Y.; Nguyen, T. *Appl. Phys. Lett* **1998,** *73*, 1514.

Yokomichi, H.; Hayashi, T. *Appl. Phys. Lett.* **1998,** *72*, 2704.

Yokomichi, H.; Hayashi, T.; Amano, T.; Masuda, A. *J. Non-Cryst. Solids* **1998,** *227-230*, 641.

Yoon, D.-S.; Baik, H. K.; Lee, S.-M. *J. Appl. Phys.* **1998,** *83*, 8074.

Yoon, D.-S.; Baik, H. K.; Lee, S.-M. *J. Vac. Sci. Technol. B* **1999,** *17*, 174.

Yun, S.-M.; Chang, H.-Y.; Kang, M.-S.; Choi, C.-K. *Thin Solid Films* **1999,** *341*, 109-111.

Zhao, B.; Feiler, D.; Ramanathan, V.; Liu, Q. Z.; Brongo, M.; Wu, J.; Zhang, H.; Kuei, J. C.; Young, D.; Brown, J.; Vo, C.; Xia, W.; Chu, C.; Zhou, J.; Nguyen, C.; Tsau, L.; Dornisch, D.; Camilletti, L.; Ding, P.; Lai, G.; Chin, B.; Krishna, N.; Johnson, M.; Turner, J.; Ritzdorf, T.; Wu, G.; Cook, L. *Electrochem. Solid-State Lett.* **1998,** *1*, 276-278.